



HAL
open science

Rheological behaviour of pure clay and coarse-grained clay suspensions using an inclined blade vane-in-cup

A. Bougouin, A. Benamar, A. Jarno, François Marin, A. Pantet

► To cite this version:

A. Bougouin, A. Benamar, A. Jarno, François Marin, A. Pantet. Rheological behaviour of pure clay and coarse-grained clay suspensions using an inclined blade vane-in-cup. *Journal of Non-Newtonian Fluid Mechanics*, 2022, 300, pp.104714. 10.1016/j.jnnfm.2021.104714 . hal-04000713

HAL Id: hal-04000713

<https://hal.science/hal-04000713>

Submitted on 22 Feb 2023

HAL is a multi-disciplinary open access archive for the deposit and dissemination of scientific research documents, whether they are published or not. The documents may come from teaching and research institutions in France or abroad, or from public or private research centers.

L'archive ouverte pluridisciplinaire **HAL**, est destinée au dépôt et à la diffusion de documents scientifiques de niveau recherche, publiés ou non, émanant des établissements d'enseignement et de recherche français ou étrangers, des laboratoires publics ou privés.

Journal Pre-proof

Rheological behaviour of pure clay and coarse-grained clay suspensions using an inclined blade vane-in-cup

A. Bougouin, A. Benamar, A. Jarno, F. Marin, A. Pantet

PII: S0377-0257(21)00190-7

DOI: <https://doi.org/10.1016/j.jnnfm.2021.104714>

Reference: JNNFM 104714

To appear in: *Journal of Non-Newtonian Fluid Mechanics*

Received date: 28 September 2021

Revised date: 23 November 2021

Accepted date: 24 November 2021

Please cite this article as: A. Bougouin, A. Benamar, A. Jarno et al., Rheological behaviour of pure clay and coarse-grained clay suspensions using an inclined blade vane-in-cup, *Journal of Non-Newtonian Fluid Mechanics* (2021), doi: <https://doi.org/10.1016/j.jnnfm.2021.104714>.

This is a PDF file of an article that has undergone enhancements after acceptance, such as the addition of a cover page and metadata, and formatting for readability, but it is not yet the definitive version of record. This version will undergo additional copyediting, typesetting and review before it is published in its final form, but we are providing this version to give early visibility of the article. Please note that, during the production process, errors may be discovered which could affect the content, and all legal disclaimers that apply to the journal pertain.

© 2021 Published by Elsevier B.V.



Rheological behaviour of pure clay and coarse-grained clay suspensions using an inclined blade vane-in-cup

A. Bougouin, A. Benamar, A. Jarno, F. Marin, A. Pantet

Laboratoire Ondes et Milieux Complexes (LOMC) - Université Le Havre Normandie, UMR 6294 CNRS, 76063 Le Havre, France

Abstract

Mixtures of clay and sand suspended in water are complex systems encountered in many industrial and environmental applications, but their understanding and modelling are still limited and require further investigations. In this way, the rheological behaviour of pure non-thixotropic clay and coarse-grained clay suspensions is investigated with a rotational rheometer equipped by an inclined blade vane-in-cup, where the type and the volume fraction of both fine clay and coarse materials are varied. The Herschel-Bulkley model $\tau = \tau_y + K\dot{\gamma}^n$ is used to describe successfully the flow curves of suspensions relating the shear stress τ to the shear rate $\dot{\gamma}$, from which the yield stress τ_y , the consistency K and the index n are deduced. The main contributions of this study are (i) to validate the inclined blade vane-in-cup for the estimation of the rheological behaviour of polymer microgels, pure clay suspensions, and coarse-grained clay suspensions, (ii) to conclude on the most appropriate model type to predict the yield stress of pure clay suspensions over a wide range of fine clay volume fractions, and (iii) to highlight how frictional contacts of coarse grains may play a role on the bulk yield stress of coarse-grained clay suspensions. We believe that this work would be useful for improving the rheological description of cohesive suspensions in geophysical and industrial applications.

Keywords: Rheology, Vane-in-cup, Yield stress, Suspension, Clay material, Coarse grains

1. Introduction

Grain-liquid mixtures may be encountered in many industrial processes (e.g., concrete, drilling mud) and environmental applications (e.g., mudflow, flood, sediment transport), and the understanding of such systems is essential to predict their ability to flow depending on grain and liquid properties, as well as the

Email addresses: alexis.bougouin@univ-lehavre.fr (A. Bougouin), ahmed.benamar@univ-lehavre.fr (A. Benamar)

6 stress conditions. Grain-liquid suspensions may exhibit a variety of complex be-
 7 haviours depending on the dominant interaction type [1]. A popular approach
 8 consists in describing the suspension as a single effective fluid at the macro-
 9 scopic scale, which is characterized by a constitutive law $\tau = f(\dot{\gamma})$ relating the
 10 shear stress τ to the shear rate $\dot{\gamma}$. In this objective, a lot of devices and tests
 11 were proposed to determine their rheological properties, such as the inclined
 12 plane test [2, 3, 4, 5], the slumping test [6, 7, 8, 9], the capillary rheometer
 13 [10], and the rotational rheometer [11, 12, 13]. The latter one is probably the
 14 most famous device because it allows to estimate the flow curve $\tau(\dot{\gamma})$ of ma-
 15 terials under well-controlled conditions. A specific attention should, however,
 16 be given to the geometry used depending on the investigated material because
 17 of experimental constraints and artefacts that may lead to a misinterpretation
 18 of results. For instance, the cone-plate is commonly used because both τ and
 19 $\dot{\gamma}$ can be expressed theoretically from the torque T and the rotational rate Ω ,
 20 while remaining quasi-homogeneous within the material. However, this geom-
 21 etry is limited to pure fluids, and eventually fine-grained suspensions, because
 22 of the small gap in which the material is sheared. Others (e.g., parallel plates,
 23 coaxial cylinders) exist each with their advantages and limitations, while more
 24 complex geometries are also developed for which the theoretical framework is
 25 hardly established, i.e. the ball measuring system [14], the fractal 3D printed
 26 vanes [15], and the inclined blade vane-in-cup [16]. In this latter case, they
 27 are rarely considered by the scientific community due to the lack of theoretical
 28 background, but they could represent alternative tools for complex materials.

29 A crude classification is usually proposed between the suspensions made of
 30 colloidal and noncolloidal materials based on a critical diameter, typically as-
 31 sessed around $50 \mu\text{m}$, below which Brownian motion, electrostatic forces and
 32 van der Waals attraction may be predominant over hydrodynamic and solid
 33 interactions [17]. In the simplest case of coarse grains suspended into a New-
 34 tonian fluid using density matching and high viscous fluids, the bulk behaviour
 35 of the suspension is broadly related to an apparent Newtonian fluid [18, and
 36 references herein]. Theoretical expressions and phenomenological models were
 37 proposed for predicting the growth of the apparent viscosity $\eta = \tau/\dot{\gamma}$ with the
 38 coarse particle volume fraction ϕ_c , whose most of them diverge at a maximum
 39 volume fraction ϕ_m above which the suspension should be jammed. It is usu-
 40 ally found in the range $\phi_m \approx [0.55 : 0.62]$ lower than the random close packing
 41 of monodisperse spherical particles (i.e., $\phi_{RCP} \approx 0.64$), which is attributed to
 42 small-range interactions between solid particles [19, 20, 21, 22]. In the case of
 43 fine and colloidal particles, the bulk behaviour of suspensions strongly differs
 44 from an apparent Newtonian fluid due to interparticle forces. Such suspensions
 45 are related to nonlinear rheological behaviours with yield stress (a minimum
 46 stress to flow), shear-thinning or shear-thickening (decrease or increase of η for
 47 increasing values of $\dot{\gamma}$, respectively), and thixotropy (time-dependency). One
 48 of the most famous examples of colloidal suspensions is probably clay-water
 49 mixtures, also referred to as muddy fluids.

50 The rheological behaviour of clay-water suspensions can be well described by
 51 the Herschel-Bulkley model $\tau = \tau_y + K\dot{\gamma}^n$, where τ_y , K and n are three fitting

52 parameters corresponding to the yield stress, the consistency, and the flow index,
 53 respectively [e.g., 23, 24]. However, some caution should be paid because K and
 54 n do not represent a specific property of suspensions [23]. In fact, the term $K\dot{\gamma}^n$
 55 is representative of viscous dissipation within the suspension, and it is expected
 56 to recover an apparent Newtonian behaviour, i.e. $\tau = \eta\dot{\gamma}$, when colloidal forces
 57 become negligible over hydrodynamic dissipation at sufficiently high shear rates
 58 [25]. By contrast, the yield stress τ_y reflects the microstructure of the suspension
 59 through the cohesion forces of clay materials. A specific interest was therefore
 60 given to the dependency of τ_y on a wide range of parameters, such as the type
 61 of clay material, the organic content, the preparation method, the shear-history,
 62 the pH, the temperature, the salinity, and the fine clay volume fraction [e.g.,
 63 26, 23, 27, 28, 29, 30, 31, 32, among others]. In particular, predictive models
 64 were proposed to relate the yield stress τ_y to the fine clay volume fraction ϕ_f .
 65 From experimental observations, an exponential law was first considered as

$$\tau_y(\phi_f) = \alpha_1 \exp(\alpha_2 \phi_f), \quad (1)$$

66 where α_1 and α_2 are two fitting parameters found in the wide range of $[7 \times 10^{-4} :$
 67 $3]$ and $[8 : 45]$, respectively [2, 25, 33, 34]. This relation can be reasonably
 68 applied for moderate-concentrated suspensions, but it does not hold true for
 69 diluted clay suspensions for which $\tau_y \sim \alpha_1$ when $\phi_f \rightarrow 0$. Semi-empirical models
 70 were then established taking into account the microstructural parameters of
 71 suspensions. The derivation of these models is also based on the idea that
 72 the yield stress vanishes and diverges at low and high fine volume fractions,
 73 respectively. This leads to the following formula

$$\tau_y(\phi_f) = \beta_1 \left(\frac{\phi_f}{\phi_m - \phi_f} \right)^{\beta_2}, \quad (2)$$

74 where β_1 and β_2 are two fitting parameters, and ϕ_m is the maximum volume
 75 fraction above which the suspension should be jammed. Equation (2) is equiv-
 76 alent to the model of Spearman [35], while it can be reduced to that of Zhou et
 77 al. [36] with $\phi_m = 1$. The Yodel model [37] was also proposed based on a single
 78 fitting parameter δ depending on particle properties, while both a percolation
 79 threshold ϕ_p and a maximum volume fraction ϕ_m are considered :

$$\tau_y(\phi_f) = \delta \frac{\phi_f^2 (\phi_f - \phi_p)}{\phi_m (\phi_m - \phi_f)}. \quad (3)$$

80 Note that this model suggests the divergence of the yield stress when $\phi_f \rightarrow \phi_p$
 81 and $\phi_f \rightarrow \phi_m$, the first one being interpreted as the minimum volume fraction
 82 ϕ_p needed to form a solid percolating network (i.e., a few percent).

83 The inclusion of coarse grains in clay suspensions, and more generally in
 84 nonlinear fluids, also affects the rheological behaviour of the bulk suspension.
 85 It is usually reported that increasing the volume fraction ϕ_c of coarse grains
 86 promotes larger yield stresses τ_y , larger apparent viscosities η (or larger consis-
 87 tencies K), and larger elastic modulus consistent with the increase of viscous

88 dissipation within the suspension [e.g., 6, 28, 38, 39, 40]. Based on a nonlinear
 89 homogenization method, Chateau et al. [41] developed a model to predict the
 90 yield stress τ_y as a function of the coarse volume fraction ϕ_c as

$$\tau_y(\phi_c)/\tau_y(0) = \sqrt{(1 - \phi_c)(1 - \phi_c/\phi_m)^{-\lambda\phi_m}}, \quad (4)$$

91 where $\tau_y(0)$ is the yield stress of the suspending fluid, e.g. the fine clay sus-
 92 pension, and $\lambda = 2.5$ is a constant parameter. For coarse spherical particles,
 93 the maximum volume fraction is found equal to $\phi_m \sim 0.56 - 0.57$ [41, 42, 43],
 94 while the polydispersity and the shape of coarse grains may affect this value
 95 [44, 45]. It is also important to remind that Eq. (4) primarily provides a
 96 good agreement with experimental data originated from local measurements,
 97 and the macroscopic determination of rheological parameters may lead to sig-
 98 nificant differences with this model [39]. Moreover, this model is established
 99 by considering a purely mechanical contribution of the coarse grains within the
 100 suspension, independently on the physicochemical properties of materials.

101 In the most specific configuration of rivers and estuaries, a fine proportion
 102 of clay materials within a non-cohesive environment may reduce drastically the
 103 sediment transport rate, which may be interpreted as a larger yield stress of the
 104 mixture. As a first step, this study aims to help improving the understanding
 105 and the assessment of constitutive laws for coarse grains in clay suspensions.
 106 The rheological behaviour of pure non-thixotropic clay and coarse-grained clay
 107 suspensions is investigated using a rotational rheometer equipped by an inclined
 108 blade vane-in-cup, where the type and the volume fraction of fine clay and coarse
 109 materials are varied. The questions raised in the present contribution are the
 110 following. Can the inclined blade vane-in-cup be used to estimate the rheological
 111 properties of clay-water mixtures containing or not coarse grains? What are the
 112 relative influence of the total solid, fine clay, and coarse volume fractions on the
 113 behaviour of suspensions? Can the rheological parameters be predicted using
 114 simple models? To provide some answers, the paper is organized as follows.
 115 In Sec. 2, the rheometer devices, the materials used, and the validity domain
 116 of rheological measurements for coarse-grained clay suspensions are presented.
 117 Then, the reliability of the inclined blade vane-in-cup is assessed by comparing
 118 the rheological measurements of Carbopol dispersions with those of a cone-plate
 119 and coaxial cylinders (Sec. 3). Finally, a fine analysis of the influence of the
 120 type and the volume fraction of both fine clay and coarse materials on the bulk
 121 behaviour of suspensions is described (Sec. 4).

122 2. Methodology

123 2.1. Rheometer devices and procedure

124 The rheological measurements are performed using both a Physica MCR
 125 501 rheometer and a RheolabQC rheometer from Anton Paar, equipped with a
 126 cone-plate (angle: 1° , radius: $R^{CP} = 25$ mm, truncated gap: $e = 99 \mu\text{m}$), and
 127 an inclined blade vane-in-cup (width gap: $R_{cup} - R_{rotor} = 12.5$ mm between the

128 cup and the rotor, $R_{cup} - R_{blade} = 2.5$ mm between the cup and the blade edge)
 129 or coaxial cylinders (width gap: $R_{cup} - R_{cylinder} = 1.1$ mm between the cup and
 130 the inner cylinder, radius and height of the inner cylinder: $R_{cylinder} = 13.3$ mm
 131 and $h_{cylinder} = 40.0$ mm), respectively. The Physica MCR 501 rheometer is
 132 equipped with a Peltier device keeping the temperature at 21° , and the cone-
 133 plate is covered by a cap to prevent evaporation because of the small sample
 134 volume used, i.e. $\sim 0.5 - 1$ mL. Most experiments are performed with the
 135 inclined blade vane-in-cup consisting of six blades located over three levels, for
 136 which the two bottom blades are inclined at 45° , rotating in a roughened cup
 137 [Figs 1(a)-(b)]. To our knowledge, this complex geometry, sometimes referred as
 138 starch stirrer cell, has only been used to characterize the rheological behaviour
 139 of starch pastes [e.g., 16, 46, 47, 48], while it may also be an appropriate tool for
 140 coarse grains in clay suspensions. In fact, the secondary flows induced by the
 141 inclined bottom blades reduce the settling of coarse grains in the suspending
 142 fluid, while the flow structure could help against shear-induced migration, for
 143 maintaining a quasi-homogeneous suspension.

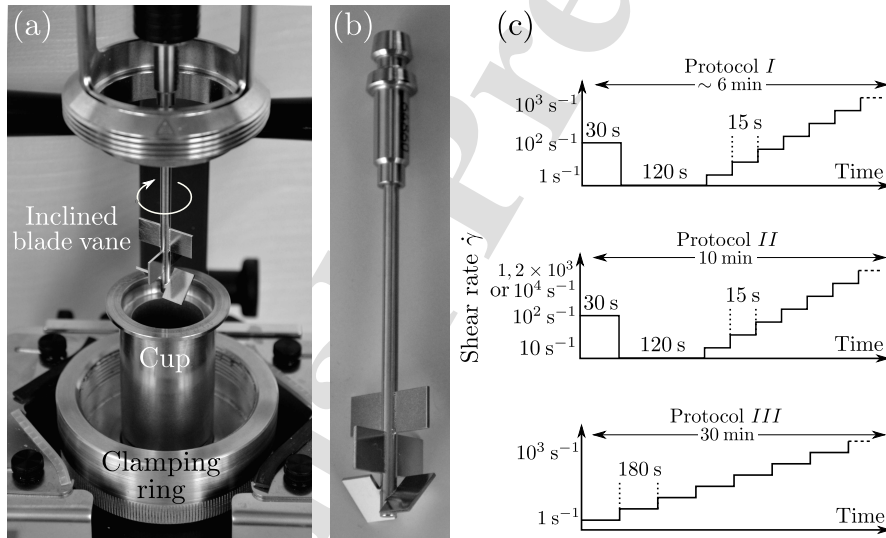


Figure 1: (a) View of the RheolabQC rheometer equipped with the inclined blade vane-in-cup [see the zoom, in (b)]. The clamping ring allows to maintain centered the cup with respect to the inclined blade vane during the rheological measurements. (c) Sketch of the three protocols of measurements used in the present study.

144 Three different procedures of measurements, referred to as protocols *I*, *II*
 145 and *III* in the following, are used to ensure the independency of the results
 146 on the experimental procedure because of the lack of standard protocols [Fig.
 147 1(c)]. Protocol *I* consists of a ‘quick’ flow curve, during which the material is
 148 pre-sheared at $\dot{\gamma} = 10^2 \text{ s}^{-1}$ for 30 seconds, then followed by a rest period of
 149 120 seconds, and finally the material is sheared by increasing the shear rate

150 logarithmically from $\dot{\gamma} = 1$ to 10^3 s^{-1} , with a measurement every 15 seconds
 151 during 225 seconds (i.e., a total of 15 measurements). Protocol *II* is defined
 152 on the same basis of protocol *I* with a pre-shearing at $\dot{\gamma} = 10^2 \text{ s}^{-1}$ for 30
 153 seconds, and a rest period of 120 seconds. Then, the shear rate is increased
 154 logarithmically from $\dot{\gamma} = 10 \text{ s}^{-1}$ to $\dot{\gamma} = 10^4$ and $1, 2 \times 10^3 \text{ s}^{-1}$ for the Physica MCR
 155 501 rheometer and the RheolabQC rheometer, respectively, with a measurement
 156 every 15 seconds during 450 seconds (i.e., a total of 30 measurements). Note
 157 that the maximum value $\dot{\gamma} = 1, 2 \times 10^3 \text{ s}^{-1}$ corresponds to the limit value of
 158 the shear rate for the RheolabQC rheometer. Finally, protocol *III* is a ‘slow’
 159 flow curve during which the shear stress τ is measured each second during 180
 160 seconds, at a given shear rate varied from $\dot{\gamma} = 1$ to 10^3 s^{-1} (a total duration
 161 of 30 minutes) without pre-shearing. Then, the shear stress τ is estimated as
 162 the average value over the last 30 seconds, at each $\dot{\gamma}$. Note that the given
 163 values of $\dot{\gamma}$ correspond to those provided by the manufacturer software, and
 164 some differences with the ‘true’ shear rate $\dot{\gamma}$ of the inclined blade vane-in-cup
 165 will be discussed in Sec. 3.

166 Finally, more details on the rheological measurements and their limitations
 167 are provided in Appendix A. In particular, the limitations caused by the technical
 168 characteristics of rheometers and the experimental artefacts are discussed
 169 to prevent a misinterpretation of results.

170 2.2. Materials

171 Suspensions are made of fine clay and coarse grains suspended in tap water.
 172 The clay materials used are illite (47% illite, 47% calcite, 6% quartz) from
 173 the Lizy-sur-Ourcq quarry, and kaolinite (67% kaolinite, 17% quartz, 16% illite)
 174 from the Ploemur quarry, both located in France, and manufactured by Argiletz
 175 and Imerys, respectively. Both types are non-thixotropic and non-swelling clay
 176 materials that prevent time and shear-history dependencies on the rheological
 177 properties of suspensions, unlike other types of clay materials (e.g., smectites)
 178 [49]. The particle size and the density are estimated as $(d_f, \rho_f) = (4_{-3}^{+10} \mu\text{m},$
 179 $2500 \pm 25 \text{ kg.m}^{-3})$ and $(7_{-5}^{+16} \mu\text{m}, 2550 \pm 30 \text{ kg.m}^{-3})$ for illite and kaolinite, respec-
 180 tively. Note that the particle size of clay materials is more representative of clay
 181 stacks formed by van der Waals attractions than individual clay sheets. Two
 182 types of coarse materials are used, namely a fine sand with $(d_c, \rho_c) = (111_{-32}^{+46} \mu\text{m},$
 183 $2650 \pm 20 \text{ kg.m}^{-3})$ and a coarse sand with $(345_{-105}^{+152} \mu\text{m}, 2620 \pm 30 \text{ kg.m}^{-3})$ from
 184 the Nemours and Hostun quarries (France), respectively, manufactured by Sil-
 185 beco, and spherical glass beads with $(d_c, \rho_c) = (247_{-68}^{+91} \mu\text{m}, 2500 \pm 30 \text{ kg.m}^{-3})$
 186 manufactured by Matrasur Composites. Both types of coarse materials may
 187 be characterized as a collection of rounded grains, which are more faceted and
 188 angular with sand materials than smooth glass beads. More details on the
 189 properties of clay and sand materials are given in Appendix B. Finally, the
 190 suspending fluid is tap water with a dynamic viscosity of $\eta_w \approx 10^{-3} \text{ Pa.s}$ and a
 191 density of $\rho_w \approx 1000 \text{ kg.m}^{-3}$.

192 A specific attention is paid to the preparation of suspensions, and it may be
 193 detailed as follows. Each suspension is first prepared by hand-mixing the clay

194 mass m_f and the water mass m_w during few minutes. The pure clay suspension
 195 is then left at rest one day before the measurements to ensure a proper hydration
 196 of the clay material. The suspension is characterized by the fine clay volume
 197 fraction (relative to the volume of water and clay material) as

$$\hat{\phi}_f = \frac{\rho_w m_f}{\rho_w m_f + \rho_f m_w}. \quad (5)$$

198 A mass m_c of coarse materials is eventually added into the suspension, and
 199 then mixed during few minutes before the measurements. In the case of glass
 200 beads, they are cleaned in an ultrasound bath during about 15 minutes and then
 201 dried in an oven prior to adding into the suspension. This process allows to
 202 avoid surface interactions that may affect drastically the rheological behaviour
 203 of suspensions, due to any remaining surfactant at the surface of the beads
 204 following the production process. In addition to the fine clay volume fraction,
 205 the coarse-grained clay suspension should be characterized by the coarse or the
 206 total solid volume fractions defined as

$$\phi_c = \frac{\rho_f \rho_w m_c}{\rho_c \rho_w m_f + \rho_f \rho_w m_c + \rho_f \rho_c m_w}, \quad (6)$$

$$\phi_t = \frac{(\rho_c m_f + \rho_f m_c) \rho_w}{\rho_c \rho_w m_f + \rho_f \rho_w m_c + \rho_f \rho_c m_w}, \quad (7)$$

207 respectively, while the fine clay volume fraction (relative to the volume of the
 208 suspension) is equal to $\phi_f = \phi_t - \phi_c$. It is important to mention that only
 209 two parameters among $\hat{\phi}_f$, ϕ_f , ϕ_c , and ϕ_t are necessary to characterize the
 210 suspension because they are related by $\phi_t = \phi_f + \phi_c$ and $\hat{\phi}_f = \phi_f / (1 - \phi_c)$.
 211 For pure clay suspensions, it is reduced to a single parameter as $\hat{\phi}_f \equiv \phi_f \equiv \phi_t$
 212 and $\phi_c = 0$. For the sake of clarity, the fine clay volume fraction $\hat{\phi}_f$, the coarse
 213 volume fraction ϕ_c , and the total solid volume fraction ϕ_t will be used in further
 214 sections. In the present study, they are varied up to $\hat{\phi}_f = 0.427$, $\phi_c = 0.576$,
 215 and $\phi_t = 0.707$, respectively.

217 Additional experiments are performed with polymer microgels of Carbopol
 218 Ultrez 10 (from Lubrizol) dispersed in purified water, which are well-known
 219 yielding and shear-thinning fluids [50]. The preparation of Carbopol dispersions
 220 needs some specific stages. Firstly, the dry powder of Carbopol is poured in
 221 water, then it is mixed with a magnetic agitator during one day, and finally the
 222 dispersion is neutralized by adding 10 mL of a sodium hydroxide solution (1M
 223 NaOH) per gram of Carbopol. The final pH of Carbopol dispersions is estimated
 224 at $\sim 7 - 8$ using an Elmetron pH-meter CP-411, while the weight concentration
 225 $C = m_{Carbopol} / (m_{Carbopol} + m_{NaOH} + m_w)$ with $m_{Carbopol}$, m_{NaOH} , and m_w
 226 the masses of Carbopol, sodium hydroxide solution, and water, respectively, is
 227 varied in the range $C = [0.1 : 1.7]\%$.

228 2.3. Domain of rheological measurements

229 First of all, it is important to determine the range of parameters for which
 230 the rheological behaviour of coarse-grained clay suspensions could be investi-

231 gated at the laboratory scale. Figure 2 shows the set of measurements per-
 232 formed in this study (circles) and those provided by the literature (crosses) for
 233 estimating the rheological parameters of coarse-grained clay suspensions, in the
 234 $([(\phi_t - \phi_c)/\phi_t, \phi_t])$ -plane. Remind that $(\phi_t - \phi_c)/\phi_t$ represents the proportion of
 235 fine clay relative to that of solid (fine and coarse) materials and ϕ_t is the total
 236 solid volume fraction relative to the suspension (see Sec. 2.2). A wide range of
 237 configurations is covered here from natural to well-controlled suspensions (e.g.,
 238 natural muddy sediments, glass beads in kaolinite suspensions) characterized
 239 by various rheological devices and tests (e.g., parallel plates, coaxial cylinders,
 240 slumping test).

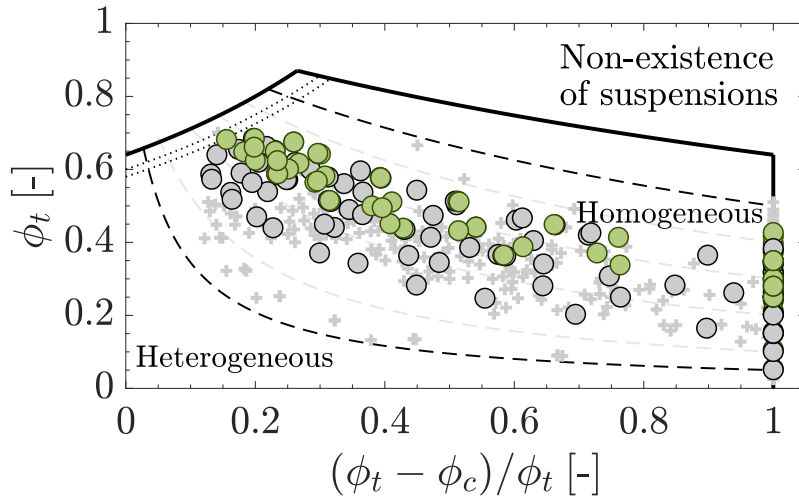


Figure 2: Domain of rheological measurements for coarse-grained clay suspensions, in the $([(\phi_t - \phi_c)/\phi_t, \phi_t])$ -plane. Circles and crosses represent the set of rheological measurements performed in this study (green circles: illite, grey circles: kaolinite) and those provided by the literature [crosses: 6, 23, 24, 33, 38, 40, 51, 52, 53, 54, 55], respectively. (—) Random close packing of bimodal systems with $\phi_t = \phi_{RCP}/(1 - (\phi_t - \phi_c)/\phi_t)$ and $\phi_t = \phi_{RCP}/[1 - (1 - (\phi_t - \phi_c)/\phi_t)(1 - \phi_{RCP})]$ below and above $(\phi_t - \phi_c)/\phi_t = 0.265$, respectively, and $\phi_{RCP} = 0.64$ is the random close packing of unimodal systems [6, 56]; (- - -) iso-values of the fine clay volume fraction $\hat{\phi}_f = 0.05, 0.1, 0.2, 0.3, 0.4, \text{ and } 0.5$ (from bottom to top); (\cdots) iso-values of the coarse volume fraction $\phi_c = 0.58$ and 0.6 (from bottom to top).

241 Firstly, the existing range of coarse-grained clay suspensions is indicated
 242 by the solid lines, in Fig. 2. In particular, the maximum total solid volume
 243 fraction ϕ_t of suspensions is limited by the random close packing of bimodal
 244 systems. When the difference in size is large enough between two types of
 245 spherical particles, the random close packing may be estimated theoretically as
 246 $\phi_t = \phi_{RCP}/(1 - (\phi_t - \phi_c)/\phi_t)$ and $\phi_t = \phi_{RCP}/[1 - (1 - (\phi_t - \phi_c)/\phi_t)(1 - \phi_{RCP})]$
 247 at low and large $(\phi_t - \phi_c)/\phi_t$, respectively [6, 56]. The random close packing of
 248 unimodal systems is set here to $\phi_{RCP} = 0.64$ commonly used for hard spherical

249 particles [57], while it is expected to be a reasonable approximation for clay
 250 stacks [35].

251 Now, the rheological measurements are practicable and reliable as long as the
 252 suspension is homogeneous during the measurement. This condition is failed
 253 when coarse grains settle significantly within the suspension, which can be at-
 254 tributed to the excess of the particle weight over the yield stress of the sus-
 255 pending clay suspension in absence of deformation [30]. As discussed in Sec. 1,
 256 the yield stress of pure clay suspensions is mainly controlled by the fine volume
 257 fraction $\hat{\phi}_f$ and the iso-values are therefore shown by dashed lines, in Fig. 2.
 258 All rheological measurements of coarse-grained clay suspensions are performed
 259 here with $\hat{\phi}_f > 0.05$ (bottom dashed line), while most of them are included in
 260 the narrow range $\hat{\phi}_f \approx [0.15 : 0.35]$. Additionally, the fine clay volume fraction
 261 never exceeds $\hat{\phi}_f = 0.5$ (top dashed line), above which the suspension is probably
 262 close to a purely solid-like behaviour at the laboratory scale. Disregarding now
 263 the clay material, heterogeneities may also be induced by the relative motion
 264 of individual coarse particles. At sufficiently high volume fractions, a granular
 265 material should dilate before flowing that causes local variations of the volume
 266 fraction [58]. This phenomenon is usually observed above a coarse volume frac-
 267 tion of $\phi_c = 0.58 - 0.6$ [59, 60, 61], which is shown by the dotted lines in Fig.
 268 2.

269 To conclude on this part, the rheological measurements of coarse-grained clay
 270 suspensions are practicable and relatively reliable in the domain delimited by the
 271 black dashed lines and the dotted lines, in which the suspensions are expected to
 272 be broadly homogeneous, at least at the initial time. Accordingly, the present
 273 study covers a wide range of volume fractions using both the cone-plate and
 274 the inclined blade vane-in-cup for pure clay suspensions, i.e. $(\phi_t - \phi_c)/\phi_t = 1$,
 275 and only the inclined blade vane-in-cup for coarse-grained clay suspensions, i.e.
 276 $(\phi_t - \phi_c)/\phi_t < 1$ (circles, in Fig. 2). However, some caution has to be exercised
 277 on this global representation because the limiting curves are dependent on the
 278 properties of clay and coarse materials used, while heterogeneities may also
 279 be caused by other physical processes (e.g., particle migration) disregarded here
 280 because of their dependency on the rheological devices and the shear conditions.

281 3. Validity of the inclined blade vane-in-cup

282 Prior to investigate the rheological behaviour of pure clay and coarse-grained
 283 clay suspensions, the flow curves of Carbopol dispersions estimated with the
 284 inclined blade vane-in-cup are compared to those of both the cone-plate and
 285 coaxial cylinders using the same protocol with the aim of assessing the reliability
 286 of rheological measurements. In particular, Carbopol dispersions represent a
 287 suitable yielding and shear-thinning fluid analogous to pure clay suspensions,
 288 while they have been intensively studied in the literature [50].

289 Contrary to both the cone-plate and coaxial cylinders, the complex shape
 290 of the inclined blade vane-in-cup does not permit to relate theoretically both
 291 the shear stress τ and the shear rate $\dot{\gamma}$ to the torque T and the rotational rate

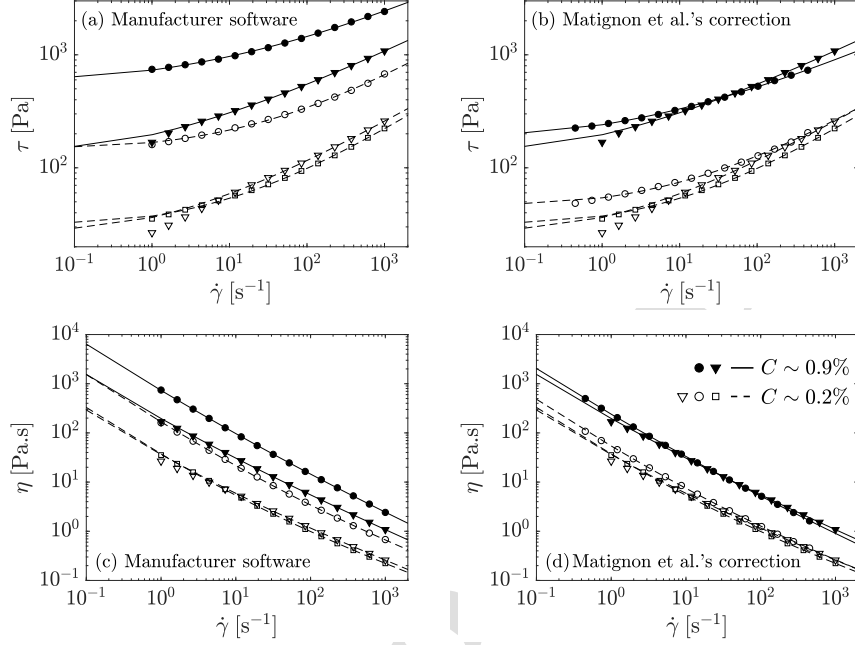


Figure 3: (a)-(b) Shear stress τ and (c)-(d) apparent viscosity η as a function of the shear rate $\dot{\gamma}$ measured by the inclined blade vane-in-cup (circles), the cone-plate (triangles), and coaxial cylinders (squares) with protocol *I*, for Carbopol dispersions with $C \sim 0.2\%$ (opened symbols, dashed lines) and $C \sim 0.9\%$ (closed symbols, solid lines). For the inclined blade vane-in-cup, the quantities are estimated as $\tau = C_1 T$, $\dot{\gamma} = C_2 \Omega$ and $\eta = \tau / \dot{\gamma} = C_1 T / C_2 \Omega$, with (a)-(c) $C_1 = 138 \text{ Pa} \cdot (\text{mN} \cdot \text{m})^{-1}$ and $C_2 = 1 \text{ min} \cdot \text{s}^{-1}$ used by the manufacturer software and (b)-(d) $C_1 = 41.7 \text{ Pa} \cdot (\text{mN} \cdot \text{m})^{-1}$ and $C_2 = 0.45 \text{ min} \cdot \text{s}^{-1}$ proposed by Matignon et al. [16]. The lines are the best fits of the Herschel-Bulkley model, i.e. (a)-(b) $\tau = \tau_y + K \dot{\gamma}^n$ and (c)-(d) $\eta = \tau_y / \dot{\gamma} + K \dot{\gamma}^{n-1}$, where τ_y , K , and n are the yield stress, the consistency, and the flow index, respectively.

292 Ω , respectively. Hence, both quantities are estimated empirically as $\tau = C_1 T$
 293 and $\dot{\gamma} = C_2 \Omega$, where $C_1 = 138 \text{ Pa} \cdot (\text{mN} \cdot \text{m})^{-1}$ and $C_2 = 1 \text{ min} \cdot \text{s}^{-1}$ are the con-
 294 version factors used by the manufacturer software. In Fig. 3(a)-(c), the flow
 295 curves of Carbopol dispersions estimated with the inclined blade vane-in-cup
 296 using the conversion factors of the manufacturer software (circles) are com-
 297 pared to those obtained with the cone-plate (triangles) and coaxial cylinders
 298 (squares) with protocol *I*, for two different weight concentrations C (opened
 299 vs. closed symbols). Note that the rheological measurements performed with
 300 the cone-plate and coaxial cylinders cannot exceed the weight concentration of
 301 $C \sim 1\%$ and 0.5% , respectively. Regardless of the geometry used, Carbopol
 302 dispersions behave as yielding and shear-thinning fluids dependent on C , as
 303 expected. However, quantitative differences may be observed between the flow
 304 curves obtained with the inclined blade vane-in-cup and those of both the cone-

305 plate and coaxial cylinders despite the same protocol used. In fact, similar
 306 conclusions have already been reported for Newtonian and shear-thinning fluids
 307 measured with both the inclined blade vane-in-cup and coaxial cylinders [16].
 308 This difference was attributed to the conversion factors used by the manufac-
 309 turer software, and Matignon et al. [16] proposed more appropriate values of
 310 $C_1 = 41.7 \text{ Pa} \cdot (\text{mN} \cdot \text{m})^{-1}$ and $C_2 = 0.45 \text{ min} \cdot \text{s}^{-1}$ based on their own calibra-
 311 tion. Figure 3(b)-(d) shows a better collapse of flow curves estimated with the
 312 three different geometries by considering the Matignon et al.'s correction [16]
 313 for the inclined blade vane-in-cup. Some slight differences can be still reported
 314 probably due to experimental artefacts related to the geometry used (e.g., ad-
 315 herence condition), but these discrepancies remain relatively low compared to
 316 those associated to the variations of different parameters considered in the fol-
 317 lowing. Finally, the flow curves of Carbopol dispersions can be well fitted (least
 318 square method, here and elsewhere) by the Herschel-Bulkley model, i.e. (a)
 319 $\tau = \tau_y + K\dot{\gamma}^n$ and (b) $\eta = \tau_y/\dot{\gamma} + K\dot{\gamma}^{n-1}$ (solid and dashed lines), from which
 320 the yield stress τ_y , the consistency K , and the flow index n are extracted.

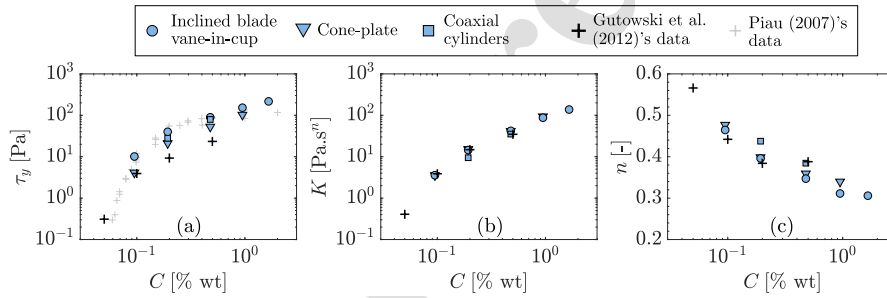


Figure 4: (a) Yield stress τ_y , (b) consistency K , and (c) flow index n estimated by the inclined blade vane-in-cup using the Matignon et al.'s correction [16] (circles), the cone-plate (triangles), and coaxial cylinders (squares) with protocol I , as a function of the weight concentration C for Carbopol dispersions. Black and grey crosses correspond to data available in the literature for Carbopol Ultrez 10 dispersions measured with a roughened cone-plate [62] and Carbopol 940 and 980 dispersions measured with different setups [50], respectively.

321 In order to strengthen the relevance of the Matignon et al.'s correction [16],
 322 Fig. 4 shows (a) the yield stress τ_y , (b) the consistency K , and (c) the flow index
 323 n estimated by the inclined blade vane-in-cup using the Matignon et al.'s cor-
 324 rection [16] (circles), the cone-plate (triangles), and coaxial cylinders (squares),
 325 as a function of the weight concentration C for Carbopol dispersions. Moreover,
 326 data available in the literature for Carbopol Ultrez 10 dispersions measured with
 327 a roughened cone-plate (black crosses) and Carbopol 940 and 980 dispersions
 328 measured with different setups (grey crosses) are also reported for comparison.
 329 Overall, both τ_y and K increase and n decreases with increasing values of C ,
 330 which is consistent with data from the literature (black and grey crosses). More-
 331 over, both K and n are in excellent agreement with data of Gutowski et al. [62]
 332 (black crosses) corresponding to Carbopol Ultrez 10 dispersions as used here.

333 Quantitative differences on the yield stress τ_y can be reported between our data
 334 and those of Gutowski et al. [62], while remaining broadly included in the typi-
 335 cal variation of Carbopol dispersions (black and grey crosses). In the following,
 336 the shear stress τ and the shear rate $\dot{\gamma}$ are still estimated from the torque T
 337 and the rotational rate Ω of the inclined blade vane-in-cup using the conversion
 338 factors proposed by Matignon et al. [16].

339 4. Application to complex suspensions

340 4.1. Rheological properties and modelling of pure clay suspensions

341 The influence of the fine clay volume fraction $\hat{\phi}_f$ on the rheological behaviour
 342 of pure clay suspensions, i.e. without coarse materials, can be now addressed
 343 using the inclined blade vane-in-cup. Some measurements are also performed
 344 with the cone-plate to cover a wider range of volume fractions. It can be re-
 345 minded that pure clay suspensions are controlled here by the type and the fine
 clay volume fraction, given that $\hat{\phi}_f \equiv \phi_t$ and $\phi_c = 0$.

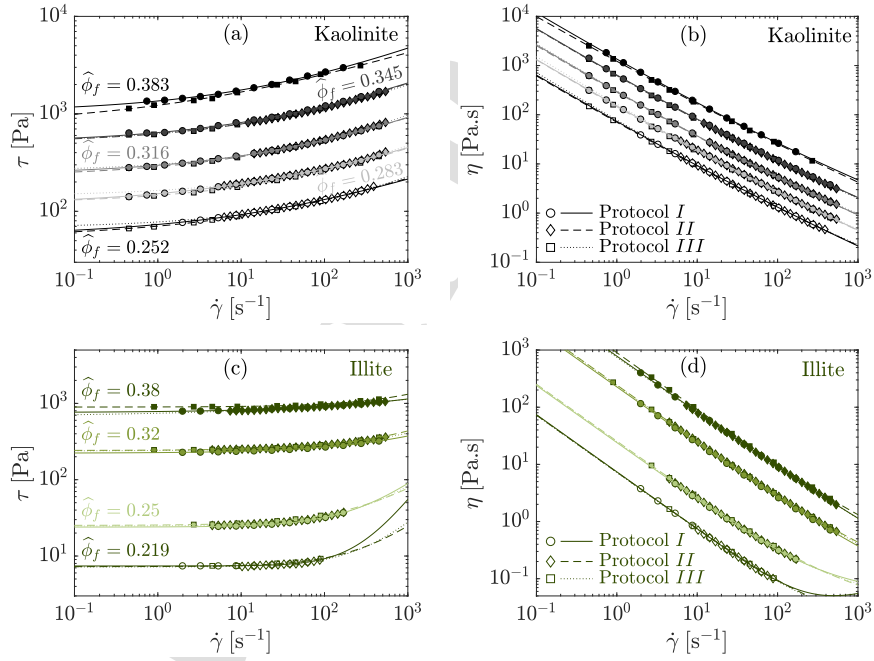


Figure 5: (a)-(c) Shear stress τ and (b)-(d) apparent viscosity η as a function of the shear rate $\dot{\gamma}$ measured by the inclined blade vane-in-cup with different protocols [see legend, in (b)-(d)], for (a)-(b) pure kaolinite suspensions and (c)-(d) pure illite suspensions with various fine clay volume fractions $\hat{\phi}_f$ ($\equiv \phi_t$, here) [see legend, in (a)-(c)]. The lines are the best fits of the Herschel-Bulkley model, i.e. (a)-(c) $\tau = \tau_y + K\dot{\gamma}^n$ and (b)-(d) $\eta = \tau_y/\dot{\gamma} + K\dot{\gamma}^{n-1}$, where τ_y , K , and n are the yield stress, the consistency, and the flow index, respectively.

346
 347 Figure 5 shows (a)-(c) the shear stress τ and (b)-(d) the apparent viscosity
 348 η as a function of the shear rate $\dot{\gamma}$ measured by the inclined blade vane-in-
 349 cup with different protocols (see symbols and lines), for pure kaolinite (grey)
 350 and pure illite (green) suspensions increasing the fine clay volume fraction $\hat{\phi}_f$
 351 (from light to dark colors). For decreasing values of the shear rate $\dot{\gamma}$, the shear
 352 stress τ tends towards a constant value and the viscosity η increases, which is
 353 consistent with a yielding and shear-thinning behaviour as expected for pure clay
 354 suspensions [63]. Moreover, one clearly observes that the dissipative behaviour
 355 of suspensions is mainly controlled by the fine clay volume fraction $\hat{\phi}_f$ due to
 356 both cohesion and viscous effects. The addition of clay materials increases the
 357 number of links between clay particles consolidating the network, while the size
 358 of interstices, in which the interstitial fluid is sheared, is reduced promoting
 359 viscous dissipation. On the other hand, the matching of the flow curves using
 360 different protocols confirms the independency of results on the experimental
 361 procedure, while quantifying the accuracy of measurements. In each case, the
 362 flow curves can be well fitted by the Herschel-Bulkley model (lines) defined as
 363 (a)-(c) $\tau = \tau_y + K\dot{\gamma}^n$ and (b)-(d) $\eta = \tau_y/\dot{\gamma} + K\dot{\gamma}^{n-1}$, from which the yield stress
 364 τ_y , the consistency K , and the flow index n are extracted. Note that similar
 365 conclusions are drawn from the flow curves of suspensions obtained with the
 366 cone-plate.

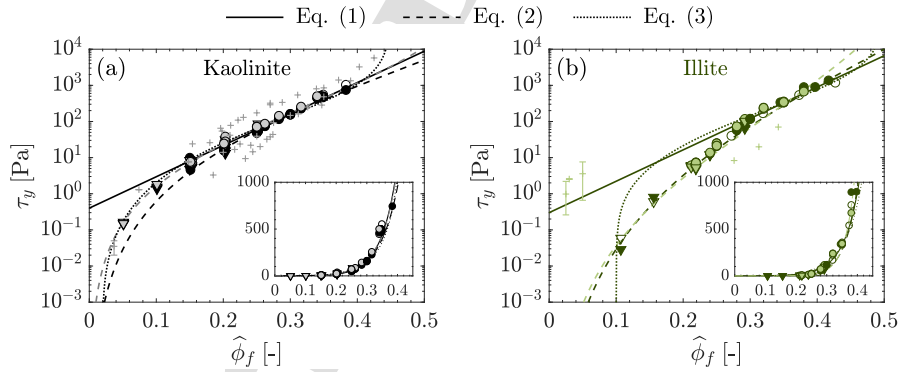


Figure 6: Yield stress τ_y as a function of the fine clay volume fraction $\hat{\phi}_f$ for (a) pure kaolinite suspensions and (b) pure illite suspensions, measured by the cone-plate (triangles) and the inclined blade vane-in-cup (circles) with protocols *I*, *II*, and *III* (from light to dark colors). Crosses are data from the literature - In (a): [6, 23, 24, 53, 54, 55]; In (b): [52, 53]. (—) Exponential law (Eq. 1) with (a) $(\alpha_1, \alpha_2) = (0.4, 20)$, and (b) $(\alpha_1, \alpha_2) = (0.3, 20)$; (- -) Zhou-Spearman model (Eq. 2) with (a) $(\beta_1, \beta_2, \phi_m) = (5 \cdot 10^3, 4.1, 1)$ (dark grey) and $(\beta_1, \beta_2, \phi_m) = (250, 3, 0.64)$ (light grey), and (b) $(\beta_1, \beta_2, \phi_m) = (10^4, 5.8, 1)$ (dark green) and $(\beta_1, \beta_2, \phi_m) = (120, 4.8, 0.64)$ (light green); (· · ·) Yodel model (Eq. 3) with (a) $(\delta, \phi_p, \phi_m) = (400, 0.02, 0.45)$, and (b) $(\delta, \phi_p, \phi_m) = (800, 0.1, 0.5)$.

367 Now, the rheological parameters extracted from the Herschel-Bulkley model
 368 can be addressed as a function of the volume fraction $\hat{\phi}_f$ of clay material. In

369 particular, Fig. 6 shows the yield stress τ_y as a function of $\hat{\phi}_f$ for (a) pure
 370 kaolinite suspensions and (b) pure illite suspensions, measured by the cone-
 371 plate (triangles) and the inclined blade vane-in-cup (circles) with protocols *I*
 372 to *III* (from light to dark colors). As previously mentioned, the protocol of
 373 measurements does not affect the results quantifying thus their accuracy, and
 374 the measurements performed with both geometries match fairly well together.
 375 Moreover, one observes that τ_y increases significantly over several decades by
 376 increasing $\hat{\phi}_f$ up to ~ 0.4 , regardless of the type of clay material. At low
 377 $\hat{\phi}_f$, a sharper increase of τ_y can be reported up to $\hat{\phi}_f \approx 0.15$ and $\hat{\phi}_f \approx 0.3$
 378 for kaolinite and illite suspensions, respectively. This could suggest threshold
 379 values for the structural modification of the network within the suspensions.
 380 For pure kaolinite suspensions, our results are broadly included in the scatter of
 381 data reported in the literature (grey crosses). It is more difficult to conclude on
 382 suspensions made of illite because there are few and less accurate data available
 383 in the literature (green crosses). Finally, it is found that the yield stress of
 384 illite suspensions is lower than that of kaolinite suspensions, at given $\hat{\phi}_f$. In
 385 the literature, it is usually reported that illite is more cohesive than kaolinite
 386 due to a larger specific surface area and a larger cation exchange capacity [64].
 387 In the present study, this reverse behaviour can be explained as both kaolinite
 388 and illite materials are not pure clays and the cohesive material (i.e., kaolinite
 389 and illite) is of a higher proportion in kaolinite material (67% kaolinite and 16%
 390 illite) than in illite material (only 47% illite).

391 Different models were proposed in the literature to predict the dependency
 392 of the yield stress τ_y on the clay volume fraction $\hat{\phi}_f$ (see Sec. 1), and they are
 393 thus confronted to our experimental data to assess their relevance. Firstly, at
 394 low $\hat{\phi}_f$, the sharp increase of τ_y with $\hat{\phi}_f$ is fairly well captured by the Zhou-
 395 Spearman model (Eq. 2) with both $\phi_m = 1$ (dark dashed lines) and $\phi_m = 0.64$
 396 (light dashed lines). By contrast, the exponential law (Eq. 1) overestimates the
 397 values of τ_y (solid lines), while the concordance of the Yodel model (Eq. 3) with
 398 data is dependent on the clay material (dotted lines). It has to be reminded
 399 that the yield stress τ_y should diverge at $\hat{\phi}_f \rightarrow 0$ recovering the Newtonian
 400 behaviour of the interstitial fluid, which is inconsistent with the exponential law.
 401 At moderate values of $\hat{\phi}_f$, the trend of different models becomes similar and all
 402 of them are in good agreement with experimental data. Finally, at large $\hat{\phi}_f$, a
 403 further sharp increase of τ_y is expected according to phenomenological models,
 404 which is attributed to the divergence of the yield stress τ_y at the maximum
 405 volume fraction ϕ_m . Unfortunately, no rheological measurements are performed
 406 above a fine clay volume fraction of $\hat{\phi}_f \approx 0.4$, which does not allow to conclude
 407 on. Further work should be dedicated to the yield stress of hyperconcentrated
 408 clay suspensions, but numerical tools would probably be required. In any case,
 409 the Zhou-Spearman model (Eq. 2) represents the most appropriate model type
 410 to predict the dependency of the yield stress on the fine clay volume fraction in
 411 the wide range of parameters considered here, for which the fitting parameters
 412 are related to the properties of clay materials. Note, however, that all models are
 413 consistent with experimental data through a linear-linear representation (insets

414 of Fig. 6).

415 Lastly, both the consistency K and the flow index n may also be extracted
 416 from the best fits of the Herschel-Bulkley model. However, these two rheological
 417 parameters are poorly constrained leading to an important scatter of results
 418 (they are not shown here). In any case, both K and n do not represent a
 419 physical property of pure clay suspensions because such materials are expected
 420 to evolve from a solid-like to an apparent Newtonian behaviour at low and high
 421 shear rates, respectively [23, 25]. Thus, both K and n only allow to describe
 422 the nonlinear transient behaviour of clay suspensions over a given range of shear
 423 rates. It can still be mentioned that the increase of $\hat{\phi}_f$ broadly promotes an
 424 increase of consistency K and a decrease of flow index n from 1 to ~ 0.3 , in the
 425 range of parameters considered here.

426 4.2. Extension for coarse-grained clay suspensions

427 The rheology of pure clay suspensions is mainly controlled by the fine volume
 428 fraction $\hat{\phi}_f$ (see Sec. 4.1), but it is expected that the inclusion of noncolloidal
 429 coarse grains also affects their rheological properties. In this case, coarse-grained
 430 clay suspensions should be characterized by two independent parameters quan-
 431 tifying the content of each material, namely the fine clay volume fraction $\hat{\phi}_f$
 432 (relative to the pure clay suspension), and the total solid volume fraction ϕ_t or
 433 the coarse volume fraction ϕ_c (see their definitions, in Sec. 2.2). In the follow-
 434 ing, the rheological behaviour of coarse-grained clay suspensions is investigated
 435 with the inclined blade vane-in-cup, for which the type and the volume fraction
 436 of both fine clay and coarse materials are varied.

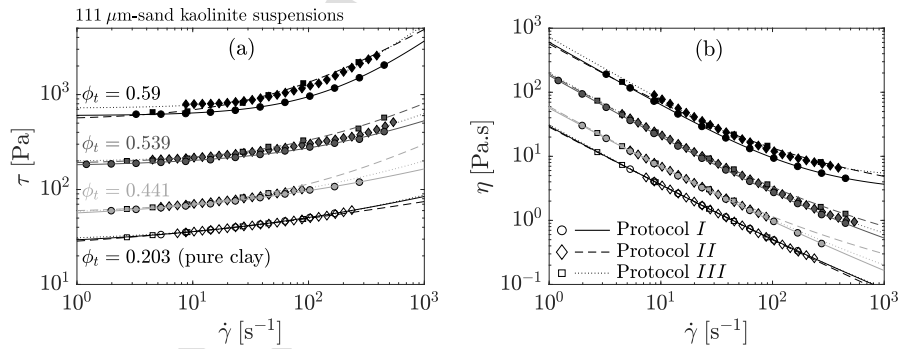


Figure 7: (a) Shear stress τ and (b) apparent viscosity η as a function of the shear rate $\dot{\gamma}$ measured by the inclined blade vane-in-cup with different protocols [see the legend, in (b)], for 111 μm -sand kaolinite suspensions with $\hat{\phi}_f = 0.203$ and various total solid volume fractions ϕ_t [see the legend, in (a)]. The lines are the best fits of the Herschel-Bulkley model, i.e. (a) $\tau = \tau_y + K\dot{\gamma}^n$ and (b) $\eta = \tau_y/\dot{\gamma} + K\dot{\gamma}^{n-1}$, where τ_y , K and n are the yield stress, the consistency, and the flow index, respectively.

437 Firstly, Fig. 7 shows the influence of the total solid volume fraction ϕ_t (i.e.,
 438 both fine clay and coarse materials) on the flow curves (a) $\tau = f(\dot{\gamma})$ and (b)

439 $\eta = f(\dot{\gamma})$ for 111 μm -sand kaolinite suspensions. Here, the fine clay volume frac-
 440 tion $\hat{\phi}_f = 0.203$ is kept constant, and the increase of ϕ_t is therefore attributed to
 441 the addition of coarse materials within the suspension. Overall, coarse-grained
 442 clay suspensions are characterized by a yielding and shear-thinning behaviour
 443 by analogy with pure clay suspensions, which is fairly well described by the
 444 Herschel-Bulkley model (lines). Moreover, the increase of ϕ_t promotes the in-
 445 crease of viscous dissipation within the suspension. It has to be reminded that
 446 the coarse material corresponds to noncolloidal solid particles not contributing
 447 to cohesion forces within the suspensions, unlike the fine clay material. It can
 448 also be reported that the similarity between the different protocols is less sat-
 449 isfactory which is mainly attributed to the accuracy of measurements, but the
 450 discrepancies remain much lower than those associated to the variations of ϕ_t .
 451 The main consequence is a poorly constrained Herschel-Bulkley model at high
 452 shear rates $\dot{\gamma}$, limiting the estimate of both the consistency K and the flow
 453 index n not considered in the following. At low shear rate $\dot{\gamma}$, however, the best
 454 fits of the Herschel-Bulkley model match fairly well for a given ϕ_t , which means
 455 that the bulk yield stress can be estimated accurately for coarse-grained clay
 456 suspensions.

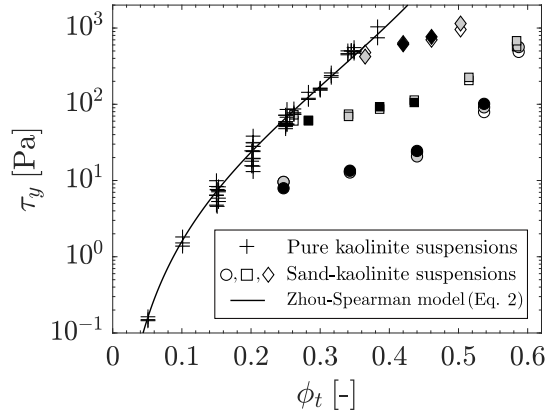


Figure 8: Yield stress τ_y as a function of the total solid volume fraction ϕ_t , for pure kaolinite suspensions (crosses) and 111 μm -sand kaolinite suspensions with $\hat{\phi}_f = 0.153$ (circles), $\hat{\phi}_f = 0.25$ (squares), and $\hat{\phi}_f = 0.34$ (diamonds) using protocols *I* to *III* (from light to dark grey). (—) Zhou-Spearman model (Eq. 2) with $(\beta_1, \beta_2, \phi_m) = (250, 3, 0.64)$.

457 In Fig. 8, the extracted yield stress τ_y of pure kaolinite suspensions (crosses)
 458 and 111 μm -sand kaolinite suspensions (other symbols) is shown as a function
 459 of the total solid volume fraction ϕ_t , in comparison. Note that crosses and
 460 the solid line correspond to the set of experiments shown in Fig. 6(a) and
 461 the Zhou-Spearman model (Eq. 2) with $(\beta_1, \beta_2, \phi_m) = (250, 3, 0.64)$ being the
 462 most appropriate model describing data of pure clay suspensions, respectively.

463 Other symbols are 111 μm -sand kaolinite suspensions with different fine clay
 464 volume fractions, i.e. $\hat{\phi}_f = 0.153$ (circles), $\hat{\phi}_f = 0.25$ (squares), and $\hat{\phi}_f = 0.34$
 465 (diamonds). One clearly observes that the trend of τ_y with ϕ_t strongly differs
 466 between both pure clay and coarse-grained clay suspensions. This highlights the
 467 different contribution of fine and coarse materials on the rheological behaviour,
 468 and more particularly, on the yield stress of suspensions. In fact, this observation
 469 could be expected because the inclusion of coarse grains mainly affects viscous
 470 dissipation, while a larger amount of fine clay material promotes cohesion and
 471 viscous dissipation within the suspension. This also supports that the yield
 472 stress τ_y of coarse-grained clay suspensions is still lower than that of pure clay
 473 suspensions at a given ϕ_t , as already reported from the slumping test for sand
 474 and glass beads in kaolinite suspensions [6].

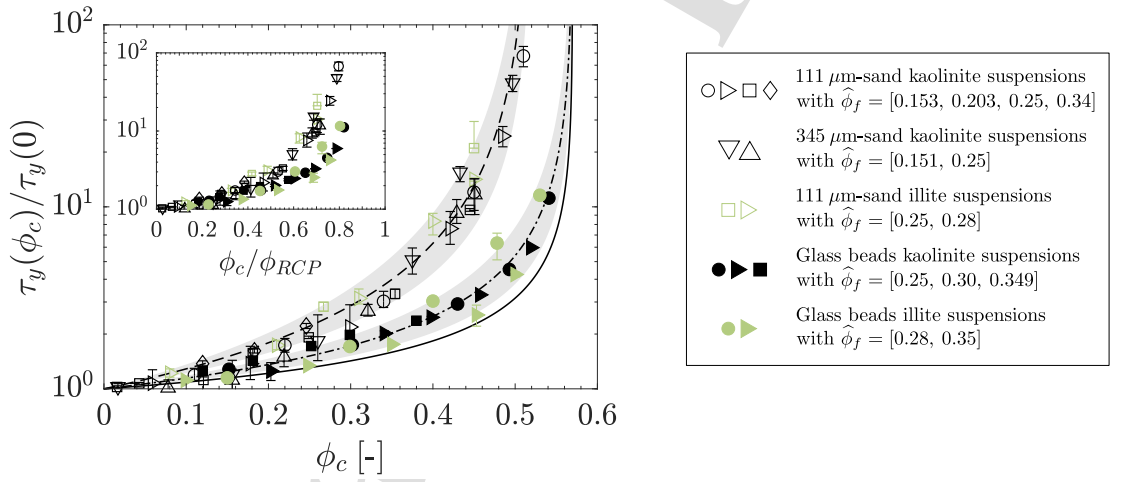


Figure 9: Yield stress $\tau_y(\phi_c)$ of coarse-grained clay suspensions normalized by the yield stress $\tau_y(0)$ of the suspending pure clay suspension, as a function of the coarse volume fraction ϕ_c (inset: as a function of ϕ_c/ϕ_{RCP} , with ϕ_{RCP} the random close packing of coarse grains). The lines and grey areas correspond to Eq. 4 with (—) $\phi_m = 0.57$ and $\lambda = 2.5$, (- - -) $\phi_m = 0.57$ and $\lambda = 3.4 \pm 0.6$, and (- · - ·) $\phi_m = 0.52$ and $\lambda = 5.5 \pm 1.0$. The values and error bars of data correspond to the average and the variation of measurements with eventually different protocols, respectively.

475 With the aim of highlighting the relative influence of coarse grains, the yield
 476 stress $\tau_y(\phi_c, \hat{\phi}_f) \equiv \tau_y(\phi_c)$ of coarse-grained clay suspensions is normalized by
 477 the yield stress $\tau_y(\phi_c = 0, \hat{\phi}_f) \equiv \tau_y(0)$ of the suspending pure clay suspension
 478 and plotted as a function of the coarse volume fraction ϕ_c , in Fig. 9. It can
 479 be first noted that the normalized yield stress $\tau_y(\phi_c)/\tau_y(0)$ increases with ϕ_c
 480 in consistence with most observations reported in the literature [6, 38, 39, 40].
 481 Moreover, this trend seems to be independent on the clay volume fraction $\hat{\phi}_f$,
 482 the type of clay material, and the mean diameter d_c of coarse materials that

483 suggests a purely mechanical contribution of coarse grains to the suspension,
 484 independently on the physicochemical properties of the materials [42, 43, 41,
 485 44, 45]. However, two different trends of $\tau_y(\phi_c)/\tau_y(0)$ may be distinguished
 486 depending on the type of coarse material, i.e. sand (opened symbols) vs. glass
 487 beads (close symbols). This difference cannot be fully attributed to the random
 488 close packing ϕ_{RCP} of coarse grains that slightly differs between sand and glass
 489 beads due to their morphology (Appendix B). In fact, the inset of Fig. 9
 490 shows that data of both coarse materials deviate significantly from each other
 491 at $\phi/\phi_{RCP} \sim 0.4 - 0.5$ (i.e., $\phi_c \sim 0.3$), above which direct particle contacts
 492 become non-negligible [19, 21, 65]. Moreover, frictional dissipation is expected
 493 to be more important with faceted and angular sand grains than with smooth
 494 spherical glass beads (see the SEM images, in Appendix B), supporting larger
 495 yield stresses of sand clay suspensions compared to glass beads clay suspensions,
 496 at a given ϕ_c .

497 A further step is to quantify the influence of coarse material types, discussed
 498 above as the contribution of particle contacts, on the bulk yield stress. In this
 499 way, the model of Chateau et al. [41] given by Eq. (4) is used because it is
 500 based on a purely mechanical contribution of coarse grains within the suspen-
 501 sion. The solid line shows Eq. 4 with $(\lambda, \phi_m) = (2.5, 0.57)$ commonly used for
 502 spherical monodisperse particles [42], in qualitative agreement with our data of
 503 glass beads in clay suspensions. Quantitative differences between the model and
 504 data may be attributed to the macroscopic approach that usually differs from
 505 local measurements [39]. Both λ and ϕ_m are therefore adjusted to obtain the
 506 best agreement between the model and experimental data, while the quantita-
 507 tive value of parameters reflects microscale interactions. In the present case, it
 508 is found $(\lambda, \phi_m) = (5.5 \pm 1.0, 0.52)$ (dashed line and grey area) for sand clay
 509 suspensions, and $(\lambda, \phi_m) = (3.4 \pm 0.6, 0.57)$ (dashed-dotted line and grey area)
 510 for glass beads clay suspensions. Note that, in the latter case, the value of ϕ_m
 511 is in agreement with that reported for spherical monodisperse beads in a yield
 512 stress fluid from local measurements [42]. Both parameters are affected by the
 513 coarse material type, and more particularly, λ increases and ϕ_m decreases when
 514 frictional contacts are expected to increase within the suspension. Similar con-
 515 clusions on both parameters have already been reported regarding numerically
 516 the power law evolution of the relative viscosity of apparent Newtonian suspen-
 517 sions varying the effective friction coefficient of grains [19, 20, 21, 22]. More
 518 recently, Blanc et al. [66] highlighted experimentally the importance of solid
 519 friction on the apparent viscosity and the jamming volume fraction of suspen-
 520 sions through shear reversal experiments of smooth spherical polystyrene beads
 521 and faceted sugar particles suspended in a Newtonian silicon oil. Hence, fric-
 522 tional contacts represent a suitable physical mechanism to explain the different
 523 trends of the yield stress with the coarse volume fraction for sand and glass
 524 beads in clay suspensions.

525 5. Conclusion

526 Rheological measurements on pure non-thixotropic clay and coarse-grained
 527 clay suspensions have been addressed using a rotational rheometer equipped
 528 with an inclined blade vane-in-cup, where the type and the volume fraction of
 529 both fine clay and coarse materials were varied. As a first step, the reliabil-
 530 ity of rheological measurements performed with the inclined blade vane-in-cup
 531 was assessed by comparing the flow curves of Carbopol dispersions with those
 532 obtained from the cone-plate and coaxial cylinders, as well as with data from
 533 the literature. It was shown that both the shear stress τ and the shear rate
 534 $\dot{\gamma}$ should be recalculated from the torque and the rotational rate using the
 535 conversion factors proposed by Matignon et al. [16], proving the deficiency
 536 of the manufacturer software that overestimates both τ and $\dot{\gamma}$ by a factor 3.3
 537 and 2.2, respectively. Then, both pure clay and coarse-grained clay suspensions
 538 were studied by extracting the rheological parameters from the Herschel-Bulkley
 539 model $\tau = \tau_y + K\dot{\gamma}^n$, with τ_y the yield stress, K the consistency, and n the flow
 540 index, fitted successfully on the flow curves $\tau = f(\dot{\gamma})$ of suspensions and inde-
 541 pendently on the protocol of measurements. The rheological behaviour of pure
 542 clay suspensions made of kaolinite and illite, was shown to be mainly controlled
 543 by the fine clay volume fraction $\hat{\phi}_f$. In particular, the yield stress τ_y increased
 544 significantly with increasing $\hat{\phi}_f$ as $\tau_y = \beta_1[\hat{\phi}_f/(\phi_m - \hat{\phi}_f)]^{\beta_2}$, where β_1 , β_2 , and
 545 ϕ_m are the fitting parameters depending on the clay materials, similar to the
 546 model type of Spearman [35] and Zhou et al. [36]. The inclusion of coarse
 547 grains in clay suspensions through the coarse volume fraction ϕ_c also increased
 548 the bulk yield stress from a purely mechanical point of view. The yield stress
 549 of the suspension relative to that of the suspending pure clay suspension was
 550 fairly well predicted as $\tau_y(\phi_c)/\tau_y(0) = \sqrt{(1 - \phi_c)(1 - \phi_c/\phi_m)^{-\lambda\phi_m}}$ based on
 551 the model type of Chateau et al. [41], where λ and ϕ_m are two fitting param-
 552 eters. Even though both parameters λ and ϕ_m differed from those commonly
 553 established for monodisperse spherical particles in a yield stress fluid from local
 554 measurements, they allowed to hold accountable for the dependency of the yield
 555 stress on the type of coarse materials attributed here to frictional contacts.

556 For the purpose of industrial and environmental applications, this study
 557 showed that the inclined blade vane-in-cup may be particularly useful to esti-
 558 mate the rheological properties of complex fluids containing coarse grains. When
 559 the field conditions prevent experimental tests, the appropriate predictive mod-
 560 els could also provide a relatively accurate estimation for the yield stress of pure
 561 clay and coarse-grained suspensions. However, future work should be dedicated
 562 to assess the dependency of fitting parameters on microscale interactions.

563 Acknowledgments

564 We are grateful to the Normandy region which has supported this work
 565 with the project RIN SELINE. We thank the support of the technical staff of
 566 the Laboratoire Ondes et Milieux Complexes (C. Houssin and M. Beaujard)
 567 for their contribution in designing and constructing mechanical pieces for the

568 RheolabQC rheometer, and S. El Maana and B. Duchemin for conducting the
 569 analysis from scanning electron microscopy (SEM) and X-ray diffraction (XRD).

570 Appendix A. Limitations of rheological measurements

571 In this section, the limitations of rheological measurements performed in this
 572 study are discussed in detail depending on both the technical characteristics
 573 of the rheometer devices and experimental artefacts. Note that the following
 574 issues are mostly attributed to the wide range of volume fractions considered
 575 from dilute to hyperconcentrated suspensions.

576 Firstly, the measuring range of the torque for the RheolabQC rheometer
 577 is broadly included between 0.1 and 75 mN.m, which prevents the rheological
 578 measurements of relatively lowly- and highly-viscous materials using the proto-
 579 cols defined in Sec. 2.1. All measurements that exceed this range are therefore
 580 unreliable and disregarded. This limitation is not reported with the Physica
 581 MCR 501 rheometer equipped by the cone-plate thanks to its wider measuring
 582 range of the torque. However, the establishment of highly-viscous or coarse-
 583 grained materials may cause an excessive normal force on the upper cone that
 584 also prevents the rheological measurements.

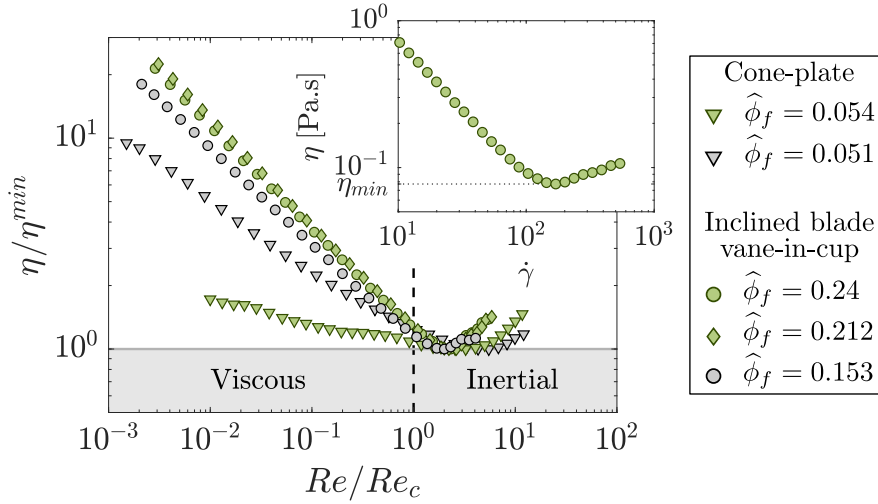


Figure A.10: Normalized apparent viscosity η/η_{min} (inset: apparent viscosity η) as a function of Re/Re_c (inset: as a function of the shear rate $\dot{\gamma}$), for pure illite suspensions (green) and pure kaolinite suspensions (grey) measured with protocol II. The Reynolds number is defined as $Re_c^{CP} = \rho R^{CP} e \dot{\gamma} / \eta$ for the cone-plate and $Re^V = \rho (R_{cup} - R_{rotor})^2 \dot{\gamma} / \eta$ for the inclined blade vane-in-cup, where $\rho = \rho_w (1 - \phi_t) + \rho_f (\phi_t - \phi_c) + \rho_c \phi_c$ ($\equiv \rho_w (1 - \hat{\phi}_f) + \rho_f \hat{\phi}_f$, here) is the bulk density of the suspension. The viscous-to-inertial flow transition is defined at a critical Reynolds number of $Re_c^{CP} = 10^3$ and $Re_c^V = 2 \times 10^2$, respectively.

585 Secondly, a viscous-to-inertial flow transition of suspensions may be observed

586 with increasing the shear rate $\dot{\gamma}$. As shown in the inset of Fig. A.10, this
 587 transition promotes an apparent shear-thickening behaviour (i.e. η increases
 588 for increasing values of $\dot{\gamma}$) of pure clay suspensions, as already reported for
 589 Newtonian fluids, shear-thinning fluids, and starch suspensions with different
 590 geometries [15, 16]. In order to overcome such a misinterpretation of results, we
 591 quantify the viscous-to-inertial flow transition by a critical Reynolds number
 592 defined according to our results as $Re_c^{CP} = \rho R^{CP} e \dot{\gamma} / \eta = 10^3$ for the cone-
 593 plate and $Re_c^V = \rho (R_{cup} - R_{rotor})^2 \dot{\gamma} / \eta = 2 \times 10^2$ for the inclined blade vane-
 594 in-cup, where $\rho = \rho_w (1 - \phi_t) + \rho_f (\phi_t - \phi_c) + \rho_c \phi_c$ is the bulk density of the
 595 suspension (Fig. A.10). Note that the critical value of Re_c^V is consistent with the
 596 criterion proposed by Matignon et al. [16], namely $\dot{\gamma} / \eta = 1662$ ($\equiv Re_c^V \approx 250$
 597 with $\rho = 1000 \text{ kg.m}^{-3}$), quantifying the viscous-to-inertial transition of various
 598 fluids using the inclined blade vane-in-cup. In the present study, the rheological
 599 measurements satisfying $Re > Re_c$ are therefore disregarded for all suspensions
 600 considered.

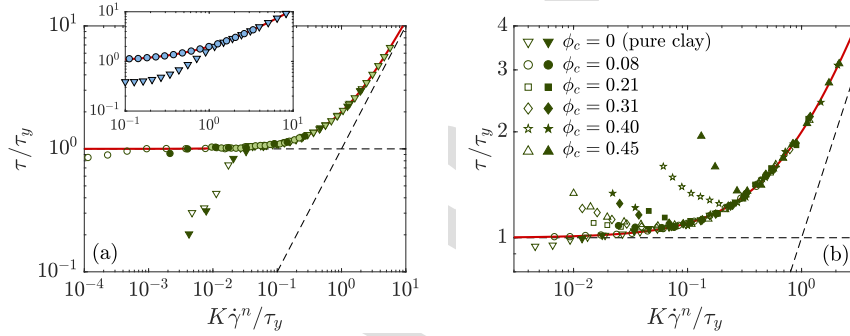


Figure A.11: Normalized shear stress τ/τ_y as a function of the normalized shear rate $K\dot{\gamma}^n/\tau_y$, for (a) pure illite suspensions with $\hat{\phi}_f \sim 0.216$ (inset: Carbopol dispersions with $C \sim 0.5\%$) measured by the cone-plate (triangles) and the inclined blade vane-in-cup (circles) with protocols *I* to *III* (from light to dark green), and (b) $111 \mu\text{m}$ -sand illite suspensions with $\hat{\phi}_f = 0.28$ and different ϕ_c (see the legend) measured by the inclined blade vane-in-cup with protocols *I* (opened symbols) and *II* (closed symbols). The solid red line corresponds to the normalized Herschel-Bulkley model $\tau/\tau_y = 1 + K\dot{\gamma}^n/\tau_y$, for which the asymptotic trends $\tau/\tau_y = 1$ and $\tau/\tau_y = K\dot{\gamma}^n/\tau_y$ are shown by the dashed lines.

601 Finally, at low $\dot{\gamma}$, some rheological measurements are not considered because
 602 they deviate surprisingly from the trend of the Herschel-Bulkley model $\tau =$
 603 $\tau_y + K\dot{\gamma}^n$, with τ_y the yield stress, K the consistency, and n the flow index.
 604 More specifically, two different trends can be reported due to different physical
 605 mechanisms (Fig. A.11). Firstly, an abrupt decrease of τ/τ_y with decreasing
 606 values of $\dot{\gamma}$ may be observed when both pure clay suspensions [Fig. A.11(a)]
 607 and Carbopol dispersions [inset of Fig. A.11(a)] are measured by the cone-
 608 plate. This is probably attributed to wall slip because both the upper cone and
 609 the bottom plate are smooth, as already reported for different types of fluids
 610 [67, 68]. By contrast, such effects are expected to be significantly reduced with

611 the inclined blade vane in a roughened cup [11], as shown in Fig. A.11(a).

612 In the case of coarse-grained clay suspensions, Fig. A.11(b) shows that a
 613 nonmonotonous trend of the shear stress τ with the shear rate $\dot{\gamma}$ may be ob-
 614 tained. More specifically, the shear stress τ first decreases and then increases
 615 with increasing $\dot{\gamma}$. The decreasing trend of the flow curve is hardly repeatable
 616 quantitatively as shown by the discrepancy between the two different proto-
 617 cols of measurements. However, this behaviour is broadly observed and more
 618 pronounced at large coarse volume fractions ϕ_c . It can be reminded that coarse-
 619 grained clay suspensions are only investigated with the inclined blade vane-in-
 620 cup, and a such behaviour cannot be reported with other geometries. In any
 621 case, the decrease of τ with increasing $\dot{\gamma}$ is usually associated to unstable flows
 622 of materials, for which the macroscopic characterization cannot reveal their real
 623 behaviour [69, 70, 71, 72]. The transition from stable to unstable flows is usually
 624 defined by a critical shear rate below which a coexistence of static and flowing
 625 regions exists. Hence, the decreasing trend of flow curves should be disregarded
 626 in order to estimate properly the rheological behaviour of suspensions.

627 Appendix B. Physical properties of materials

628 The grain size distribution of fine clay and coarse materials is measured with
 629 a Malvern Mastersizer 2000 analyser and shown in Fig. B.12. For the clay ma-
 630 terials, the measurements are performed with (light colors) and without (dark
 631 colors) an ultrasonic bath for 10 seconds beforehand, but no significant differ-
 632 ences are observed here. Remind that the elementary sheet of clay materials
 633 is usually found in the range of $10^{-1} - 10^1 \mu\text{m}$ in length and $10^{-1} - 10^0 \text{nm}$
 634 thick [6, 24, 73]. Thus, the reported value of grain size is more representative of
 635 the mean diameter of clay stacks formed by van der Waals attractions. In the
 636 present study, kaolinite and coarse materials (i.e., sand and glass beads) have
 637 an unimodal distribution, while illite material is characterized by a bimodal
 638 distribution. The two different grain sizes can be clearly visualized when illite
 639 is rehydrated after being air-dried, as shown by the picture of Fig. B.12(b). By
 640 contrast, such an observation is not reported when the suspension is initially
 641 prepared by mixing tap water and illite powder. In the following, the grain size
 642 distribution of different materials used is characterized by the diameters d_{10} ,
 643 d_{50} , and d_{90} , for which 10%, 50%, and 90% of the total volume of grains is
 644 below, respectively.

645 Secondly, a specific attention has been paid to the estimate of the density
 646 of different materials used to provide an accurate value of the fine clay, coarse
 647 and total solid volume fractions of the suspensions. In this way, the procedure
 648 consists in pouring a granular mass m_p^1 into a graduated cylinder filled with tap
 649 water [Fig. B.13(a)]. Then, the cylinder is gently tapped to release trapped air
 650 by compacting the granular material. The volume V_p^1 of particles is measured
 651 from the displaced volume of water, and this stage is repeated several times until
 652 to reach a constant value of the estimated density $\rho = m_p/V_p^1$ [see the dashed
 653 lines, in Fig. B.13(b)]. This procedure also allows to determine the maximum

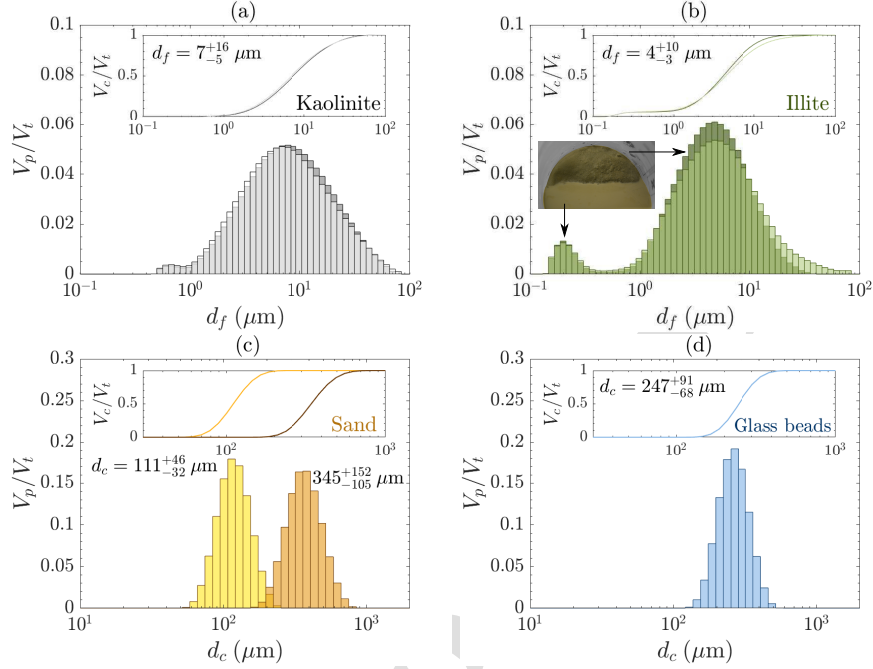


Figure B.12: Grain size distribution (inset: cumulative size distribution) of fine clay materials, namely (a) kaolinite and (b) illite, and coarse materials, namely (c) sand and (d) glass beads, where V_p , V_c , and V_t are the volume, the cumulative volume, and the total volume of grains, respectively. For the clay materials, the measurements are performed with (light colors) and without (dark colors) an ultrasonic bath for 10 seconds beforehand. The given values of the grain size correspond to the diameters d_{10} , d_{50} , and d_{90} , for which 10%, 50%, and 90% of the total volume of grains is below, respectively.

654 random packing of coarse materials by measuring the apparent volume of com-
 655 pacted grains at the end. Here, it is found equal to $\phi_{RCP} = 0.64$, 0.63, and 0.66
 656 for 111 μm -sand, 345 μm -sand and glass beads, respectively.

657 To conclude, the size and the density of fine clay and coarse materials used
 658 in the present study can be summarized as $(d_f, \rho_f) = (4_{-3}^{+10} \mu\text{m}, 2500 \pm 25$
 659 $\text{kg}\cdot\text{m}^{-3})$ and $(7_{-5}^{+16} \mu\text{m}, 2550 \pm 30 \text{ kg}\cdot\text{m}^{-3})$ for illite and kaolinite, respectively,
 660 $(d_c, \rho_c) = (111_{-32}^{+46} \mu\text{m}, 2650 \pm 20 \text{ kg}\cdot\text{m}^{-3})$ and $(345_{-105}^{+152} \mu\text{m}, 2620 \pm 30 \text{ kg}\cdot\text{m}^{-3})$
 661 for the two types of sand material, and $(d_c, \rho_c) = (247_{-68}^{+91} \mu\text{m}, 2500 \pm 30 \text{ kg}\cdot\text{m}^{-3})$
 662 for glass beads.

663 The typical morphologies of clay stacks, sand materials and glass beads are
 664 investigated using scanning electron microscopy (SEM), as shown in Fig. B.14.
 665 As mentioned above, both clay materials, namely kaolinite [Fig. B.14(a)] and
 666 illite [Fig. B.14(b)], are composed of stacks formed by van der Waals attractions
 667 with a wide variety of sizes and shapes. Here, the stacks of illite are broadly
 668 smaller than those of kaolinite, which is consistent with the lower grain size

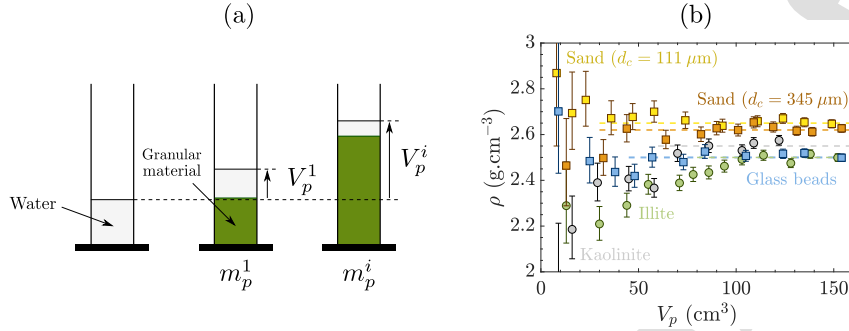


Figure B.13: (a) Sketch of the procedure for estimating the density of fine clay and coarse materials. (b) Estimated density $\rho = m_p/V_p$ of materials as a function of the total added volume V_p of particles into the graduated cylinder. The dashed lines indicate the density of each material used.

669 reported for illite compared to that of kaolinite, i.e. $d_f = 4_{-3}^{+10}$ and 7_{-5}^{+16} μm for
 670 illite and kaolinite, respectively. Moreover, smaller clay stacks are attributed to
 671 lower cohesion forces between clay particles that support the lower yield stress
 672 τ_y of pure illite suspensions compared to that of pure kaolinite suspensions, as
 673 concluded in Sec. 4.1. By contrast, the coarse materials (i.e., sand and glass
 674 beads) are characterized by a collection of individual solid grains [Fig. B.14(c)-
 675 (e)]. The sphericity $S = 2\sqrt{\pi A}/P$, with A and P the area and the perimeter
 676 of individual grains, is estimated at $S \sim 0.9$ for the sand material and $S = 1$
 677 for spherical glass beads [74]. Moreover, the two sizes of sand material may
 678 be defined as faceted and angular grains, which contrasts with spherical and
 679 smooth glass beads.

680 References

- 681 [1] P. Coussot, C. Ancey, Rheophysical classification of concentrated suspen-
 682 sions and granular pastes, *Phys. Rev. E* 59 (1999) 4445.
- 683 [2] P. Coussot, S. Boyer, Determination of yield stress fluid behaviour from
 684 inclined plane test, *Rheol. Acta* 34 (1995) 534–543.
- 685 [3] P. Coussot, S. Proust, C. Ancey, Rheological interpretation of deposits of
 686 yield stress fluids, *J. NonNewton. Fluid Mech.* 66 (1996) 55–70.
- 687 [4] S. Jarny, N. Roussel, R. Le Roy, P. Coussot, Thixotropic behavior of fresh
 688 cement pastes from inclined plane flow measurements, *Appl. Rheol.* 18
 689 (2008) 14251:1–8.
- 690 [5] C. Bonnoit, T. Darnige, E. Clement, A. Lindner, Inclined plane rheometry
 691 of a dense granular suspension, *J. Rheol.* 54 (2010) 65–79.

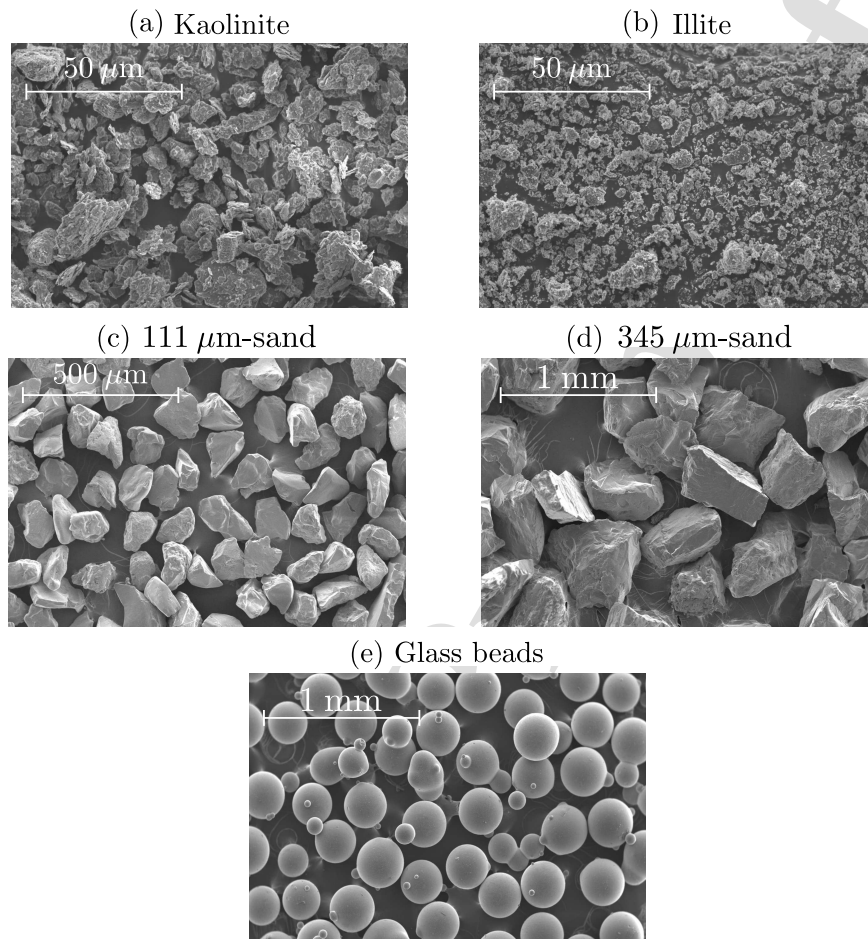


Figure B.14: Images of fine clay and coarse materials used from scanning electron microscopy (SEM).

- 692 [6] C. Ancey, H. Jorrot, Yield stress for particle suspensions within a clay
693 dispersion, *J. Rheol.* 45 (2001) 297–319.
- 694 [7] J.-C. Baudez, F. Chabot, P. Coussot, Rheological interpretation of the
695 slump test, *Appl. Rheol.* 12 (2002) 133–141.
- 696 [8] N. J. Balmforth, R. V. Craster, P. Perona, A. C. Rust, R. Sassi, Viscoplastic
697 dam breaks and the Bostwick consistometer, *J. NonNewton. Fluid Mech.*
698 142 (2007) 63–78.
- 699 [9] A. Bougouin, L. Lacaze, T. Bonometti, Collapse of a neutrally buoyant sus-

- 700 pension column: from Newtonian to apparent non-Newtonian flow regimes,
701 J. Fluid Mech. 826 (2017) 918–941.
- 702 [10] R. Alfani, N. Grizzuti, G. L. Guerrini, G. Lezzi, The use of the capillary
703 rheometer for the rheological evaluation of extrudable cement-based mate-
704 rials, Rheol. Acta 46 (2007) 703–709.
- 705 [11] H. A. Barnes, Q. D. Nguyen, Rotating vane rheometry - a review, J. Non-
706 Newton. Fluid Mech. 98 (2001) 1–14.
- 707 [12] P. J. Cullen, C. P. O'donnell, M. Houška, Rotational rheometry using com-
708 plex geometries - a review, J. Texture stud. 34 (2003) 1–20.
- 709 [13] H. A. Barnes, D. Bell, Controlled-stress rotational rheometry: An historical
710 review, Korea-Aust. Rheol. J. 15 (2003) 187–196.
- 711 [14] M. Schatzmann, G. R. Bezzola, H.-E. Minor, E. J. Windhab, P. Fischer,
712 Rheometry for large-particulated fluids: analysis of the ball measuring sys-
713 tem and comparison to debris flow rheometry, Rheol. Acta 48 (2009) 715–
714 733.
- 715 [15] C. E. Owens, A. J. Hart, G. H. McKinley, Improved rheometry of yield
716 stress fluids using bespoke fractal 3D printed vanes, J. Rheol. 64 (2020)
717 643–662.
- 718 [16] A. Matignon, F. Ducept, J.-M. Sieffermann, P. Barey, M. Desprairies,
719 S. Mauduit, C. Michon, Rheological properties of starch suspensions us-
720 ing a rotational rheometer fitted with a starch stirrer cell, Rheol. Acta 53
721 (2014) 255–267.
- 722 [17] J. M. Valverde, A. Castellanos, Random loose packing of cohesive granular
723 materials, Europhys. Lett. 75 (2006) 985.
- 724 [18] O. Pouliquen, E. Guazzelli, Rheology of dense granular suspensions, J.
725 Fluid Mech. 852 (2018) P1.
- 726 [19] S. Gallier, E. Lemaire, F. Peters, L. Lobry, Rheology of sheared suspensions
727 of rough frictional particles, J. Fluid Mech. 757 (2014) 514–549.
- 728 [20] R. Mari, R. Seto, J. F. Morris, M. M. Denn, Shear thickening, frictionless
729 and frictional rheologies in non-Brownian suspensions, J. Rheol. 58 (2014)
730 1693–1724.
- 731 [21] W. Chèvremont, B. Chareyre, H. Bodiguel, Quantitative study of the rhe-
732 ology of frictional suspensions: Influence of friction coefficient in a large
733 range of viscous numbers, Phys. Rev. Fluids 4 (2019) 064302.
- 734 [22] L. Lobry, E. Lemaire, F. Blanc, S. Gallier, F. Peters, Shear thinning in
735 non-brownian suspensions explained by variable friction between particles,
736 J. Fluid Mech. 860 (2019) 682–710.

- 737 [23] P. Coussot, J.-M. Piau, On the behavior of fine mud suspensions, *Rheol.*
738 *Acta* 33 (1994) 175–184.
- 739 [24] A. Pantet, P. Monnet, Liquid–solid transition of kaolinite suspensions,
740 *Mech. Mater.* 39 (2007) 819–833.
- 741 [25] P. Coussot, Structural similarity and transition from Newtonian to non-
742 Newtonian behavior for clay-water suspensions, *Phys. Rev. Lett.* 74 (1995)
743 3971–3974.
- 744 [26] S. H. Chang, M. H. Ryan, R. K. Gupta, The effect of pH, ionic strength,
745 and temperature on the rheology and stability of aqueous clay suspensions,
746 *Rheol. Acta* 32 (1993) 263–269.
- 747 [27] G.-Z. Xu, Y.-F. Gao, Y. Zhang, R.-B. Sun, Rheological behavior of dredged
748 slurries at high water contents, *Mar. Georesources Geotechnol.* 35 (2017)
749 357–364.
- 750 [28] V. B. Q. Nguyen, H.-S. Kang, Y.-T. Kim, Effect of clay fraction and water
751 content on rheological properties of sand–clay mixtures, *Environ. Earth*
752 *Sci.* 77 (2018) 1–9.
- 753 [29] A. Shakeel, A. Kirichek, C. Chassagne, Is density enough to predict the
754 rheology of natural sediments?, *Geo-Mar. Lett.* 39 (2019) 427–434.
- 755 [30] A. Shakeel, A. Kirichek, C. Chassagne, Effect of pre-shearing on the steady
756 and dynamic rheological properties of mud sediments, *Mar. Pet. Geol.* 116
757 (2020) 104338.
- 758 [31] J. Yin, M.-M. Hu, G.-Z. Xu, W.-X. Han, Y.-H. Miao, Effect of salinity
759 on rheological and strength properties of cement-stabilized clay minerals,
760 *Mar. Georesources Geotechnol.* 38 (2020) 610–620.
- 761 [32] Y. Lin, H. Qin, J. Guo, J. Chen, Study on the rheological behavior of a
762 model clay sediment, *J. Mar. Sci. Eng.* 9 (2021) 81:1–9.
- 763 [33] J. S. O’Brien, P. Y. Julien, Laboratory analysis of mudflow properties, *J.*
764 *Hydraul. Eng.* 114 (1988) 877–887.
- 765 [34] J. Xu, A. Huhe, Rheological study of mudflows at Lianyungang in China,
766 *Int. J. Sed. Res.* 31 (2016) 71–78.
- 767 [35] J. Spearman, An examination of the rheology of flocculated clay suspen-
768 sions, *Ocean Dyn.* 67 (2017) 485–497.
- 769 [36] Z. Zhou, M. J. Solomon, P. J. Scales, D. V. Boger, The yield stress of
770 concentrated flocculated suspensions of size distributed particles, *J. Rheol.*
771 43 (1999) 651–671.
- 772 [37] R. J. Flatt, P. Bowen, Yodel: A yield stress model for suspensions, *J. Am.*
773 *Ceram. Soc.* 89 (2006) 1244–1256.

- 774 [38] A. Pantet, S. Robert, S. Jarny, S. Kervella, Effect of coarse particle volume
775 fraction on the yield stress of muddy sediments from Marennes Oléron Bay,
776 *Adv. Mater. Sci. Eng.* 2010 (2010) 245398.
- 777 [39] G. Ovarlez, F. Mahaut, S. Deboeuf, N. Lenoir, S. Hormozi, X. Chateau,
778 Flows of suspensions of particles in yield stress fluids, *J. Rheol.* 59 (2015)
779 1449–1486.
- 780 [40] A. M. Pellegrino, L. Schippa, A laboratory experience on the effect of grains
781 concentration and coarse sediment on the rheology of natural debris-flows,
782 *Environ. Earth Sci.* 77 (2018) 749.
- 783 [41] X. Chateau, G. Ovarlez, K. L. Trung, Homogenization approach to the
784 behavior of suspensions of noncolloidal particles in yield stress fluids, *J.*
785 *Rheol.* 52 (2008) 489–506.
- 786 [42] F. Mahaut, X. Chateau, P. Coussot, G. Ovarlez, Yield stress and elastic
787 modulus of suspensions of noncolloidal particles in yield stress fluids, *J.*
788 *Rheol.* 52 (2008) 287–313.
- 789 [43] F. Mahaut, S. Mokeddem, X. Chateau, N. Roussel, G. Ovarlez, Effect
790 of coarse particle volume fraction on the yield stress and thixotropy of
791 cementitious materials, *Cem. Concr. Res.* 38 (2008) 1276–1285.
- 792 [44] T.-S. Vu, G. Ovarlez, X. Chateau, Macroscopic behavior of bidisperse sus-
793 pensions of noncolloidal particles in yield stress fluids, *J. Rheol.* 54 (2010)
794 815–833.
- 795 [45] H. Hafid, G. Ovarlez, F. Toussaint, P. H. Jezequel, N. Roussel, Effect of
796 particle morphological parameters on sand grains packing properties and
797 rheology of model mortars, *Cem. Concr. Res.* (2016) 44–51.
- 798 [46] H. E. Oh, Y. Hemar, S. G. Anema, M. Wong, D. N. Pinder, Effect of
799 high-pressure treatment on normal rice and waxy rice starch-in-water sus-
800 pensions, *Carbohydr. Polym.* 73 (2008) 332–343.
- 801 [47] H. E. Oh, Y. Pinder, Hemar, D. N., S. G. Anema, M. Wong, Effect of high-
802 pressure treatment on various starch-in-water suspensions, *Food Hydrocoll.*
803 22 (2008) 150–155.
- 804 [48] A. Pérez-Gallardo, L. A. Bello-Pérez, B. García-Almendárez,
805 G. Montejano-Gaitán, G. Barbosa-Cánovas, C. Regalado, Effect of
806 structural characteristics of modified waxy corn starches on rheological
807 properties, film-forming solutions, and on water vapor permeability,
808 solubility, and opacity of films, *Starch-Stärke* 64 (2012) 27–36.
- 809 [49] S. Yang, K. H. Andersen, Thixotropy of marine clays, *Geotech. Test. J.* 39
810 (2016) 331–339.

- 811 [50] J.-M. Piau, Carbopol gels: Elastoviscoplastic and slippery glasses made of
812 individual swollen sponges: Meso- and macroscopic properties, constitutive
813 equations and scaling laws, *J. NonNewton. Fluid Mech.* 144 (2007) 1–29.
- 814 [51] T. Iltstad, A. Elverhøi, D. Issler, J. G. Marr, Subaqueous debris flow be-
815 haviour and its dependence on the sand/clay ratio: a laboratory study
816 using particle tracking, *Mar. Geol.* 213 (2004) 415–438.
- 817 [52] A. E. James, D. J. A. Williams, P. R. Williams, Direct measurement of
818 static yield properties of cohesive suspensions, *Rheol. Acta* 26 (1987) 437–
819 446.
- 820 [53] K. L. Konan, C. Peyratout, M. Cerbelaud, A. Smith, J.-P. Bonnet,
821 A. Jacquet, Influence of two dispersants on the rheological behavior of
822 kaolin and illite in concentrated calcium hydroxide dispersions, *Appl. Clay*
823 *Sci.* 42 (2008) 252–257.
- 824 [54] A. Pierre, A. Perrot, A. Histace, S. Gharsalli, E. H. Kadri, A study on
825 the limitations of a vane rheometer for mineral suspensions using image
826 processing, *Rheol. Acta* 56 (2017) 351–367.
- 827 [55] L. Brezzi, F. Gabrieli, S. Cola, Collapse of granular–cohesive soil mixtures
828 on a horizontal plane, *Acta Geotech.* 15 (2020) 695–714.
- 829 [56] P. Gondret, L. Petit, Dynamic viscosity of macroscopic suspensions of bi-
830 modal sized solid spheres, *J. Rheol.* 41 (1997) 1261–1274.
- 831 [57] F. Zamponi, Packings close and loose, *Nature* 453 (2008) 606–607.
- 832 [58] O. Reynolds, Experiments showing dilatancy, a property of granular mate-
833 rial, possibly connected with gravitation, *Proc. R. Inst.* 11 (1886) 12.
- 834 [59] M. Pailha, M. Nicolas, O. Pouliquen, Initiation of underwater granular
835 avalanches: Influence of the initial volume fraction, *Phys. Fluids* 20 (2008)
836 111701.
- 837 [60] L. Rondon, O. Pouliquen, P. Aussillous, Granular collapse in a fluid: Role
838 of the initial volume fraction, *Phys. Fluids* 23 (2011) 073301.
- 839 [61] N. Gravish, D. I. Goldman, Effect of volume fraction on granular avalanche
840 dynamics, *Phys. Rev. E* 90 (2014) 032202.
- 841 [62] I. A. Gutowski, D. Lee, J. R. de Bruyn, B. J. Frisken, Scaling and
842 mesostructure of carbopol dispersions, *Rheol. Acta* 51 (2012) 441–450.
- 843 [63] P. Coussot, *Mudflow rheology and dynamics*, Routledge, 2017.
- 844 [64] J. H. Baas, M. L. Baker, J. Malarkey, S. J. Bass, A. J. Manning, J. A.
845 Hope, J. Peakall, I. D. Lichtman, L. Ye, A. G. Davies, D. R. Parsons,
846 D. M. Paterson, P. D. Thorne, Integrating field and laboratory approaches
847 for ripple development in mixed sand–clay–EPS, *Sedimentology* 66 (2019)
848 2749–2768.

- 849 [65] B. Vowinckel, E. Biegert, E. Meiburg, P. Aussillous, E. Guazzelli, Rheology
850 of mobile sediment beds sheared by viscous, pressure-driven flows, *J. Fluid*
851 *Mech.* 921 (2021) A20.
- 852 [66] F. Blanc, E. d'Ambrosio, L. Lobry, F. Peters, E. Lemaire, Universal scaling
853 law in frictional non-brownian suspensions, *Phys. Rev. Fluids* 3 (2018)
854 114303.
- 855 [67] S. P. Meeker, R. T. Bonnecaze, M. Cloitre, Slip and flow in pastes of soft
856 particles: Direct observation and rheology, *J. Rheol.* 48 (2004) 1295–1320.
- 857 [68] P. Ballesta, G. Petekidis, L. Isa, W. C. K. Poon, R. Besseling, Wall slip and
858 flow of concentrated hard-sphere colloidal suspensions, *J. Rheol.* 56 (2012)
859 1005–1037.
- 860 [69] G. Ovarlez, S. Rodts, X. Chateau, P. Coussot, Phenomenology and physical
861 origin of shear localization and shear banding in complex fluids, *Rheol. Acta*
862 48 (2009) 831–844.
- 863 [70] A. Kaci, M. Chaouche, P. A. Andreani, H. Brossas, Rheological behaviour
864 of render mortars, *Appl. Rheol.* 19 (2009) 13794.
- 865 [71] P. Schall, M. Van Hecke, Shear bands in matter with granularity, *Ann. Rev.*
866 *Fluid Mech.* 42 (2010) 67–88.
- 867 [72] G. Ovarlez, S. Cohen-Addad, K. Krishan, J. Goyon, P. Coussot, On the
868 existence of a simple yield stress fluid behavior, *J. NonNewton. Fluid Mech.*
869 193 (2013) 68–79.
- 870 [73] G. Varga, The structure of kaolinite and metakaolinite, *Epitoanyag* 59
871 (2007) 6–9.
- 872 [74] L. Li, M. Iskander, Evaluation of dynamic image analysis for characterizing
873 granular soils, *Geotech. Test. J.* 43 (2019) 1149–1173.

- Rheological measurements on various pure clay and coarse-grained clay suspensions
- The inclined blade vane estimates well the rheology of complex fluids with grains
- The yield stress of suspensions can be quantified using the appropriate models
- The type of coarse materials affects the yield stress due to frictional contacts

Journal Pre-proof

Declaration of interests

The authors declare that they have no known competing financial interests or personal relationships that could have appeared to influence the work reported in this paper.

The authors declare the following financial interests/personal relationships which may be considered as potential competing interests:

Journal Pre-proof